

**Discovery and Optimization of Allosteric Inhibitors
of Mutant Isocitrate Dehydrogenase 1 (R132H IDH1)
Displaying Activity in Human Acute Myeloid Leukemia Cells**

Stuart Jones, Jonathan Ahmet, Kelly Ayton, Matthew David Ball, Mark Cockerill, Emma E. Fairweather, Nicola Hamilton, Paul Harper, James R. Hitchin, Allan M. Jordan, Colin W. Levy, Ruth Lopez, Edward McKenzie, Martin J Packer, Darren Plant, Iain Simpson, Peter Simpson, Ian Sinclair, Tim C. P. Somerville, Helen Small, Gary J. Spencer, Graeme J. Thomson, Michael Tonge, Ian D. Waddell, Jarrod Walsh, Bohdan Waszkowycz, Mark Wigglesworth, Dan Wiseman, and Donald J. Ogilvie

J. Med. Chem., **Just Accepted Manuscript** • DOI: 10.1021/acs.jmedchem.6b01320 • Publication Date (Web): 15 Nov 2016

Downloaded from <http://pubs.acs.org> on November 16, 2016

Just Accepted

"Just Accepted" manuscripts have been peer-reviewed and accepted for publication. They are posted online prior to technical editing, formatting for publication and author proofing. The American Chemical Society provides "Just Accepted" as a free service to the research community to expedite the dissemination of scientific material as soon as possible after acceptance. "Just Accepted" manuscripts appear in full in PDF format accompanied by an HTML abstract. "Just Accepted" manuscripts have been fully peer reviewed, but should not be considered the official version of record. They are accessible to all readers and citable by the Digital Object Identifier (DOI®). "Just Accepted" is an optional service offered to authors. Therefore, the "Just Accepted" Web site may not include all articles that will be published in the journal. After a manuscript is technically edited and formatted, it will be removed from the "Just Accepted" Web site and published as an ASAP article. Note that technical editing may introduce minor changes to the manuscript text and/or graphics which could affect content, and all legal disclaimers and ethical guidelines that apply to the journal pertain. ACS cannot be held responsible for errors or consequences arising from the use of information contained in these "Just Accepted" manuscripts.



1
2
3
4
5
6
7
8
9
10
11
12
13
14
15
16
17
18
19
20
21
22
23
24
25
26
27
28
29
30
31
32
33
34
35
36
37
38
39
40
41
42
43
44
45
46
47
48
49
50
51
52
53
54
55
56
57
58
59
60

	Ogilvie, Donald; Cancer Research UK Manchester Institute, Drug Discovery

SCHOLARONE™
Manuscripts

Discovery and Optimization of Allosteric Inhibitors of Mutant Isocitrate Dehydrogenase 1 (R132H IDH1) Displaying Activity in Human Acute Myeloid Leukemia Cells

Stuart Jones,^{†, ∞} Jonathan Ahmet,^{†, ∞} Kelly Ayton,[†] Matthew Ball,[#] Mark Cockerill,[†] Emma Fairweather,[†] Nicola Hamilton,[†] Paul Harper,[‡] James Hitchin,[†] Allan Jordan,^{, †} Colin Levy,[#] Ruth Lopez,[#] Eddie McKenzie,[#] Martin Packer,[§] Darren Plant,[‡] Iain Simpson,[§] Peter Simpson,[‡] Ian Sinclair,[‡] Tim C. P. Somerville,[⊥] Helen Small,[†] Gary J. Spencer,[⊥] Graeme Thomson,[†] Michael Tonge,[‡] Ian Waddell,[†] Jarrod Walsh,[‡] Bohdan Waszkowycz,[†] Mark Wigglesworth,[‡] Dan Wiseman[⊥] and Donald Ogilvie[†]*

[†]Cancer Research UK Manchester Institute, Drug Discovery Unit, University of Manchester, Wilmslow Road, Withington, Manchester, M20 4BX, UK

[⊥]Cancer Research UK Manchester Institute, Leukaemia Biology Laboratory, University of Manchester, Wilmslow Road, Withington, Manchester, M20 4BX, UK

[‡]Discovery Sciences, AstraZeneca, Alderley Park, Cheshire, SK10 4TG, UK

[§]Oncology iMED, AstraZeneca, Alderley Park, Cheshire, SK10 4TG, UK

[#]Manchester Institute of Biotechnology, University of Manchester, Princess Street, Manchester, M1 7DN, UK

ABSTRACT:

A collaborative high throughput screen of 1.35 million compounds against mutant (R132H) isocitrate dehydrogenase IDH1 led to the identification of a novel series of inhibitors. Elucidation of the bound ligand crystal structure showed that the inhibitors exhibited a novel binding mode in a previously identified allosteric site of IDH1 (R132H). This information guided the optimization of the series yielding submicromolar enzyme inhibitors with promising cellular activity. Encouragingly, one compound from this series was found to induce myeloid differentiation in primary human IDH1 R132H AML cells *in vitro*.

Introduction

The enzyme isocitrate dehydrogenase 1 (IDH1) is a Nicotinamide adenine dinucleotide phosphate (NADP⁺)-dependent dehydrogenase which catalyzes the conversion of isocitrate to α ketoglutarate (α -KG). Mutations have been found in both IDH1 (R132H) and IDH2 (R140Q, R172K, R172M) in several cancer types including up to 70% of low grade and secondary glioma cases and up to 10% of acute myeloid leukemia cases.¹⁻⁴ IDH1 has been found to be frequently mutated in its active site at residue arginine 132 to histidine (R132H). This mutation leads to a loss of the normal enzymatic activity of IDH1 and the acquisition of a neomorphic activity, the conversion of α -ketoglutarate to 2-hydroxyglutarate (2-HG)⁵⁻⁷. 2-HG is considered to be an “oncometabolite” which accumulates to high levels and competitively inhibits α -ketoglutarate-dependent enzymes, such as histone demethylases and TET2, which mediates DNA

demethylation. There is an increasing body of research to investigate the effect of inhibition of IDH1 R132H on the cancer disease state⁸⁻¹³

A number of inhibitors of IDH1 R132H have been reported,¹⁴⁻²⁴ (Figure 1). Crystal structures of IDH1 R132H containing isocitrate (ICT) have provided some understanding of the change of function of the enzyme.²⁵ Of the reported IDH1 R132H inhibitors, a number have associated crystallographic data and these may be separated into two distinct classes – those that occupy the active site of the protein^{16, 21, 22} such as **2** and **4** (Figure 1) and those that occupy a remote allosteric site which then renders the protein inactive through conformational change such as **3** and **6**.^{20, 23}

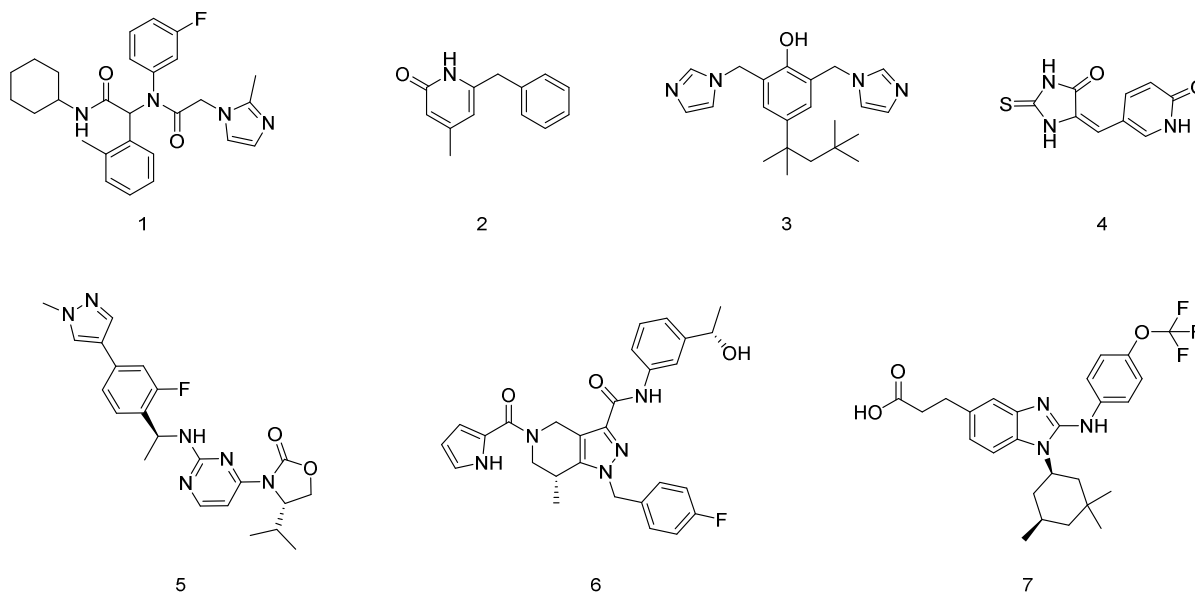


Figure 1. Examples of chemotypes reported as inhibitors of IDH1 (R132H) AGI 5198 **1**^{14, 15}, Pyridone **2**^{16, 21}, Sanofi Bisimidazole **3**²⁰, Thiohydantoin **4**²², Novartis Inhibitor **5**¹⁸, GSK321 **6**²³, Bay 1436032 **7**²⁴.

As part of the AstraZeneca (AZ) Open Innovation initiative, the Cancer Research UK Manchester Institute (CRUK-MI) and AZ entered into a collaboration to screen IDH1 (R132H)

against the AZ compound collection. A high-throughput screen (HTS) of approximately 1.35 million compounds was undertaken against the R132H mutant form of IDH1 in order to identify novel chemical matter for development as inhibitors.

The results of HTS screening (see Figure 2 for screening cascade) are described below.

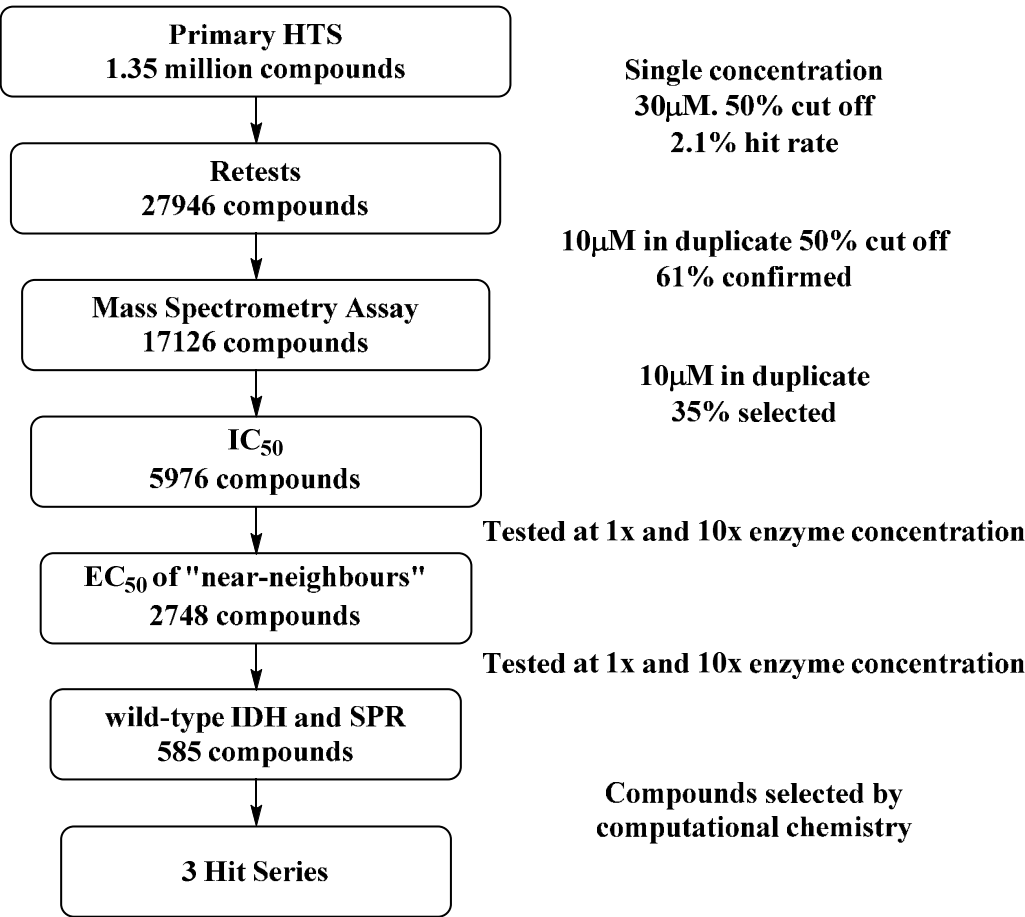


Figure 2. Screening cascade used to identify hit series from 1.35M compounds

The primary HTS performed well with a mean Z' of 0.58 and generated an initial hit rate of 2.1% using a cut off of 50% inhibition at 30 μM compound concentration in the IDH1 R132H biochemical assay. Compounds were then retested at a lower concentration (10 μM) resulting in 61.3% of hits at 30 μM reconfirming (17126 compounds). False positives (e.g. those that

interfered with the assay detection system), were identified using an orthogonal mass spectrometry assay leaving 50.5% confirmed as active. Prior to IC₅₀ determination confirmed actives were subjected to cluster analysis and virtual chemical filtering (to remove potential reactive and assay interference compounds) resulting in the selection of 5976 compounds alongside 2748 'near neighbors' for 10 point dose response determination. In order to further improve the quality of the hit output, compounds were tested in a ratio assay, i.e. testing at 1× and 10× enzyme concentration to identify any additional assay interference compounds. Compounds showing a greater than 0.5 log₁₀ shift in IC₅₀ were removed from further testing, the majority of these showing a decrease in potency under the 10x standard enzyme concentration conditions, potentially due to redox cycling or colloidal aggregation.

After these measures, further clustering by substructural analysis and Tanimoto similarity gave 585 compounds of interest, with IC₅₀ values ranging from 0.3 to 30 μM. These compounds were tested against wild-type IDH1 in a biochemical assay to determine whether the compounds were selective for the mutant isoform. None of the compounds tested showed significant activity against wild-type IDH1.

In parallel, compounds were also examined in a surface plasmon resonance (SPR) assay to confirm direct binding to the IDH R132H enzyme. Compounds that bound with a 1:1 stoichiometry were prioritized for further exploration (data not shown).

The overall result from the described screening cascade and triaging process was that compounds belonging to 3 distinct chemical series were identified for further evaluation. Previously we had found that the IDH1 (R132H) biochemical assay was sensitive to a number of metal contaminants including palladium, potentially giving rise to false positives. Several other hits,

which had used palladium in a late stage of their synthesis, were re-synthesized with particular care taken to eliminate any potential contamination of the products with residual palladium by the use of a palladium scavenger (Quadrapure® MPA) and purification of reaction products by both normal and reverse phase chromatography. However, one hit series did not use palladium in the synthetic route and examples were resynthesized in-house without these additional precautions.

On testing the in-house prepared compounds in the IDH1 R132H biochemical assay only this palladium-free series reconfirmed strongly suggesting that contamination of the original HTS samples (potentially by palladium) was responsible for the false positive response. The results for the one remaining series are shown in Table 1.

Table 1. Activity of original and resynthesized hits

Compound	Structure	Biochemical IC ₅₀ μM ^a	
		Library sample	Resynthesized
8		10.1 (0.66)	7.6 (3.7)
9		2.3 (0.20)	2.2 (0.62)
10		3.0 (n/a)	1.6 (0.04)
11		1.63 (0.07)	1.4 (0.64)

^aIC₅₀s are mean values of a minimum of 2 replicates. Standard deviations are listed in parentheses.

Compounds from this chemical series have previously been reported by AZ as inhibitors of 11β-hydroxysteroid dehydrogenase Type 1 (11β-HSD1)²⁶ offering us the opportunity to rapidly

examine additional near neighbors of the original hits, sourced from the AZ compound collection.

The preliminary SAR obtained in this manner suggested that the molecule could be simplified. Thus, the hydroxyadamantyl-amide group was replaced with cyclohexyl-amide and the sulphur linkage replaced by an ether linkage with no loss of enzyme potency, e.g. compound **12** (Figure 3).

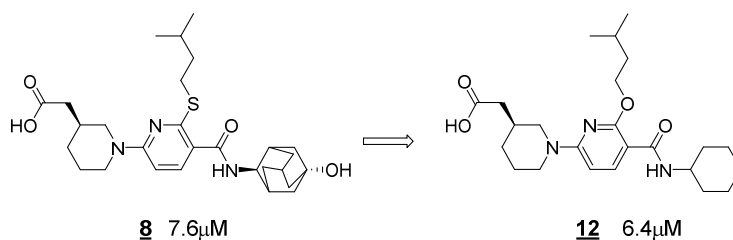


Figure 3 IDH1 (R132H) IC_{50} (μM) data for selected near neighbor of hit compound **8**.

As an aid to guide optimization, attempts were made early in the project to determine the binding mode of the initial hits using X-ray crystallography. The crystal structure of compound **9** complexed with IDH1 (R132H) homodimer in the presence of NADPH (PDB submission code 5L58) was obtained at 3.0 Å resolution (Figure 4). Although several loop regions proved to be highly disordered at this resolution, the crystal structure revealed that the unit cell contained a symmetrical dimer of (R132H) IDH1 in an “open” conformation⁵, with electron density for compound **9** and the NADP cofactor found in both protomer subunits.

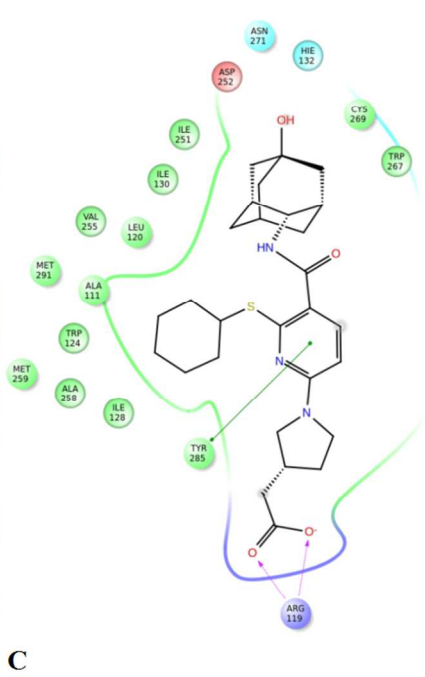
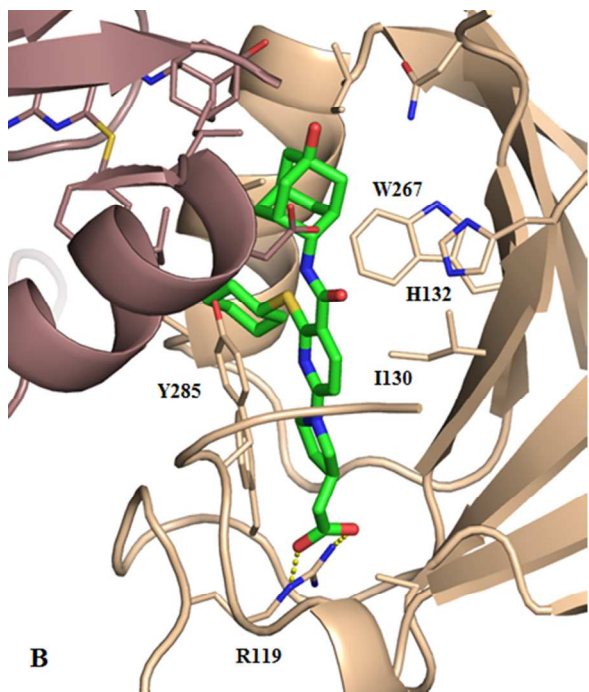
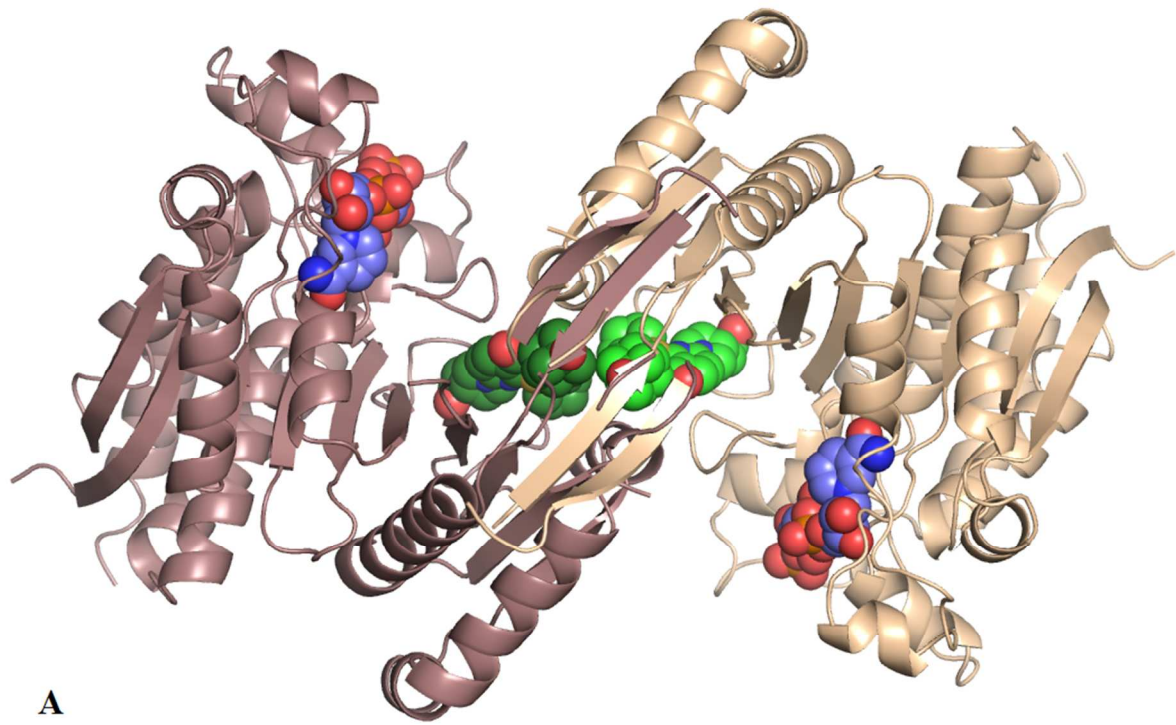


Figure 4. (A) Symmetrical dimer of (R132H) IDH1 in an “open” conformation⁵, with compound **9** (green carbons) and the NADP cofactor (blue carbons) bound in both subunits (PDB accession code 5L58) (B) Crystal structure of compound **9** bound at the dimer interface of IDH1 (R132H), with the two protomers distinguished by ribbon colour. (C) Protein:ligand interaction diagram (hydrogen bonds indicated by magenta arrows, aromatic stacking interactions by green vectors).

The inhibitor occupies a binding site at the dimer interface in a similar region to that described previously for other allosteric inhibitors.^{20, 23}. This binding site is distinct from the substrate and co-factor binding sites, with the closest distance between **9** and NADP⁺ being approximately 14 Å. Notably, the packing of the two protomers differs significantly between our crystal structure and the structure of (R132H) IDH bound to α -ketoglutarate (PDB 3INM⁵), with considerable disruption of the helical dimer interface, in particular with the helix N271 to Y285 being completely disordered.

The binding interactions around **9** are mainly lipophilic in nature, with the only direct protein hydrogen bonds arising from an ionic interaction between the carboxylic acid of compound **9** and Arg119. The central pyridine ring is pi-stacked with the side chain of Tyr285. The pyridyl 2-cyclohexylthio group occupies a discrete lipophilic pocket bounded by the residues, Trp124 and Trp 267 of chain A, and Val255 and Met259 of chains A and B. The -NH- of the pyridine 3-carboxamide potentially forms a hydrogen bond with the 2-pyridyl sulfur atom, which may serve to constrain the ligand conformation. While the sidechain of R132H is located close to the substrate binding site in the α -ketoglutarate-bound crystal structure 3INM (where it presumably modulates the neomorphic catalytic activity), in our structure it has rotated approximately 5Å away from the substrate site and towards compound **9**. Although the 3-carboxamide carbonyl group of **9** points towards R132H, it appears too distant for direct hydrogen bonding. However, the recruitment of R132H to form part of the binding cavity, away from the catalytic site, offers some explanation as to the loss of neomorphic activity in the presence of these compounds. The

pendant hydroxy adamantyl group is sited in an area which is largely unresolved (the residues Tyr272-Val281 are missing in the electron density) giving only partial structural information. The adamantyl moiety appears loosely bound although it makes several lipophilic contacts with Ile251^A, Ile251^B, Val255^B and Trp267^A. The hydroxyl group is positioned close to the sidechain of Asn271 but does not appear to make any direct hydrogen bonds.

Examination of the X-ray crystal structure suggested a number of avenues for the rapid exploration of the SAR (Figure 5).

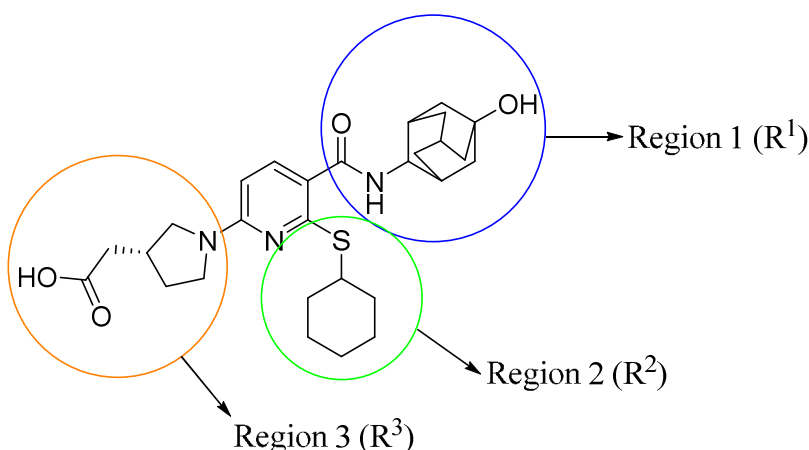


Figure 5. Potential opportunities for SAR exploration

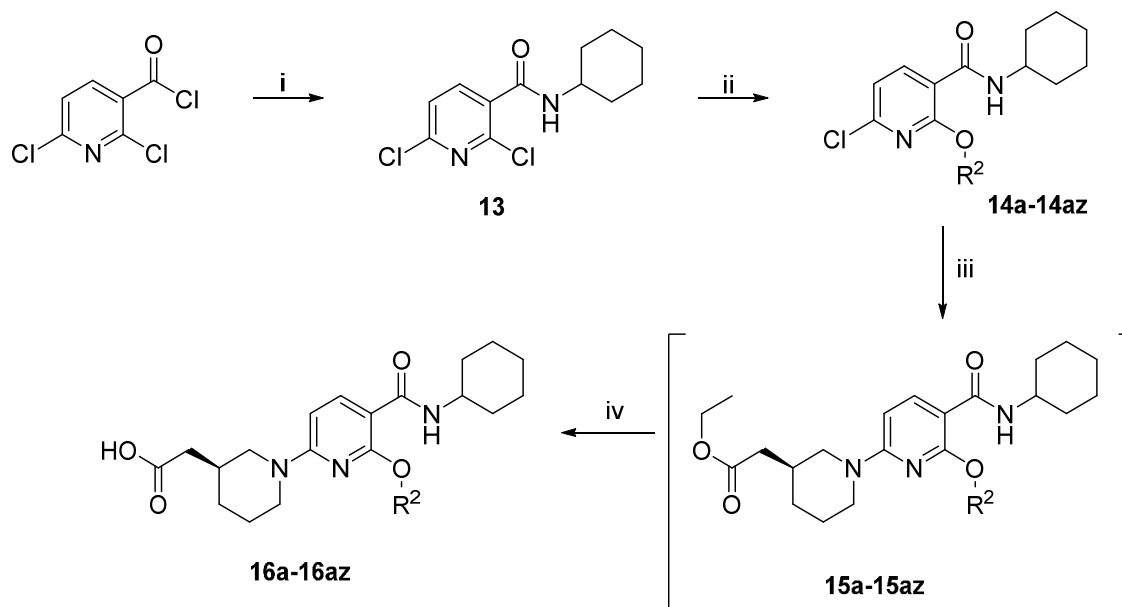
Thus for Region 1 (R¹), the potential for hydrogen bonding between the pyridyl carbonyl and the protein could be explored, alongside attempts to increase potency by finding additional contacts in the large pocket currently occupied by the hydroxy adamantyl group. The crystal structure shows that the pocket occupied by the -S-cyclohexyl moiety, Region 2 (R²), is a discrete lipophilic pocket and is likely to respond to the precise nature and shape of any ‘small’ substituents. The effects of changes to the linkage could also be explored. Region 3 (R³) is dominated by the charged interaction between the carboxylic acid and Arg119. However the

linkage between the carboxylic acid and the pyridyl ring offers scope for exploration. It was imagined that modification of each of the areas in the molecule in turn would give an understanding of the component SAR which may allow a rationale for the design of molecules with acceptable in vitro and in vivo DMPK properties, alongside improvements in selectivity against 11 β -HSD1.

CHEMISTRY

A series of compounds allowing simple substitution at the 2-position of the central pyridine (R²) were prepared with the 3-carboxamide function held as cyclohexyl and the 6-carboxylic acid function was maintained as (S)-2-(piperidin-3-yl)acetic acid using the methods shown in Scheme 1.

Scheme 1. Route to R² substituted compounds

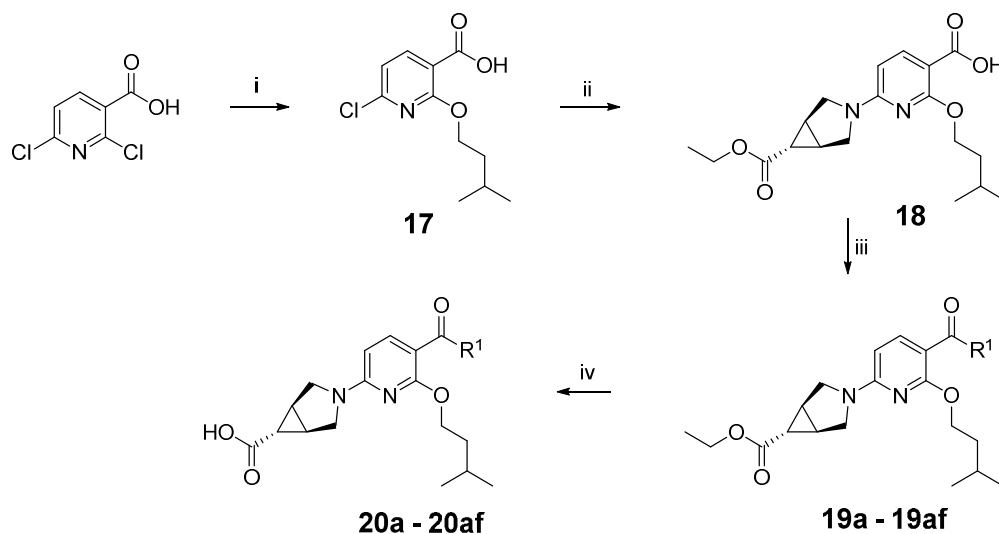


Reagents and conditions: i. Cyclohexylamine, DIPEA, DCM, RT. ii. RXH, NaH/DMF RT, 22-99%, or potassium t-butoxide /THF RT, 38-99%. iii. Ethyl (S)-2-(piperidin-3-yl)acetate, DIPEA/PrCN, 110 °C, 23-99%. iv. NaOH/MeOH rt-50 °C, 4-99%

2,6-Dichloronicotinoyl chloride was condensed with cyclohexylamine in dichloromethane (DCM) in the presence of diisopropylethylamine (DIPEA) to give 2,6-dichloro-N-cyclohexylnicotinamide **13** as a key intermediate. Displacement of the 2-chloro group was accomplished using the appropriate alcohols and either sodium hydride in DMF or potassium *tert*-butoxide in THF to give the 2-O-substituted 6-chloro-N-cyclohexyl nicotinamides **14a-az**. The regiochemistry of this reaction was confirmed for R = -O-isopentyl by removal of the remaining chlorine atom by hydrogenation and examination of the ¹H NMR aryl region for characteristic coupling patterns. The 6-chloro group was then displaced by ethyl (S)-2-(piperidin-3-yl)acetate using potassium carbonate in butyronitrile at 110 °C to give the intermediate esters **15a-az** which were hydrolysed to the acid using aqueous sodium hydroxide in methanol to give the carboxylic acids **16a-az**. The final ester hydrolysis step was frequently carried out on unpurified isolated esters allowing expedient production of final compounds.

Compounds designed to explore the SAR around the 3-carboxamide group, R1, were prepared either by the sequential route shown in Scheme 1 above (although steps were ‘telescoped’ by taking crude isolated products into the next reaction and using preparative HPLC to isolate the final product in a suitable purity) or using an alternative route which was developed to be more efficient, as shown in Scheme 2.

Scheme 2. Route to R1 substituted compounds



Reagents and conditions: i. Sodium hydride 60% in mineral oil, THF/DCM, 3-methyl butan-2-ol, RT, 73%. ii. DIPEA/PrCN 110 °C, 42-75%. iii. Aq NaOH, methanol or dioxane.

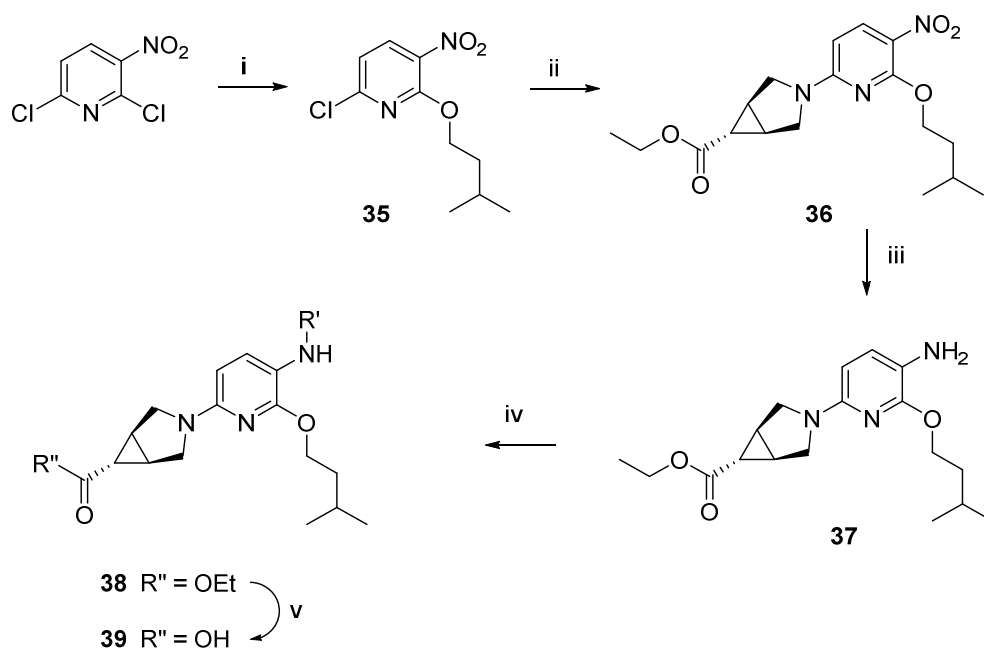
6-Chloro-2-(isopentyloxy)nicotinic acid **17** was prepared by reaction of 2,6-dichloronicotinic acid with isopentanol, (confirmation of the regiochemistry of the alkoxide addition was again obtained by removal of the remaining chlorine atom by hydrogenolysis and examination of the ^1H NMR aryl region for characteristic coupling patterns). Condensation of the amino-ester ethyl (1R,5S,6R)-3-azabicyclo[3.1.0]hexane-6-carboxylate (an alternative amino-acid function that had been identified in the original hit set) using conditions previously described followed by hydrolysis of the ester with sodium hydroxide gave the target compounds **20a-ae**. The latter two steps were combined without purification of the intermediate ester product.

Compounds bearing alternative carboxylic acid groups were prepared either using similar methods as described above (**21 – 23**) or by using Suzuki or Buchwald–Hartwig chemistry (**24 –**

28). (For these examples particular care was taken to remove residual palladium from final compounds to avoid apparent activity due to metal contamination).

Reverse carboxamide compounds **39a** – **39c** were prepared from the appropriately substituted aminopyridine compound **37** as shown in Scheme 3 using cyclohexane carboxylic acid chloride, cyclohexylisocyanate and cyclohexane sulfonyl chloride as electrophiles.

Scheme 3. Route to 3-amino substituted compounds

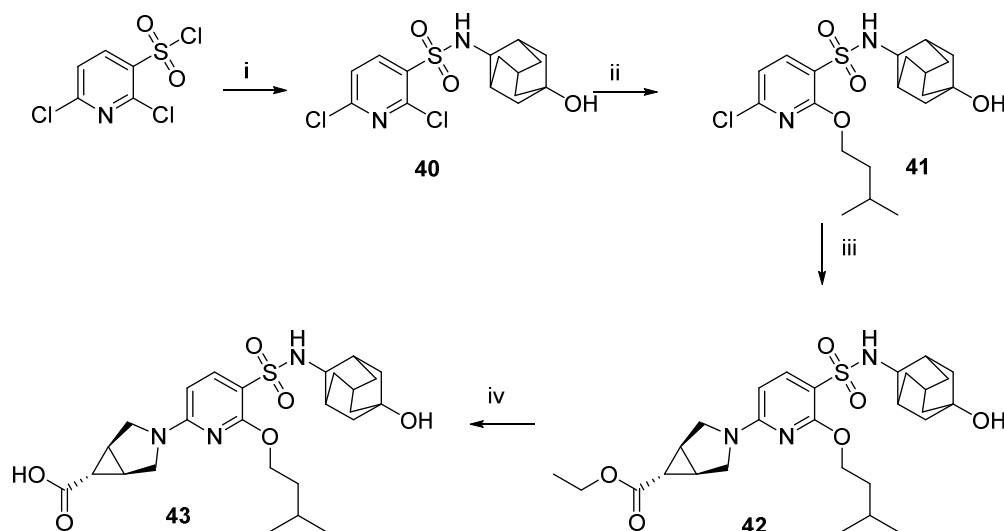


Reagents: i. 3-Methyl butanol, NaH, THF, rt, 93%. ii. Amine, DIPEA, butyronitrile, 100 °C, 75%. iii. Fe, NH₄Cl, aq. ethanol, reflux, 74%. iv. Acyl chloride, sulfonyl chloride or isocyanate, rt, 73-86%. v. Aq NaOH in methanol, rt, 38-85%.

Thus, sequential displacements of halogen from 2,5-dichloro-3-nitropyridine by isopentoxide and ethyl (1R,5S,6R)-3-azabicyclo[3.1.0]hexane-6-carboxylate followed by reduction to the amine gave intermediate **37** which was then substituted further before hydrolysis to the carboxylic acid.

Sulfonamide replacement compound **43** was prepared from 2,6-dichloropyridine-3-sulfonyl chloride as shown in Scheme 4.

Scheme 4. Route to 3-sulfonamide compound 43.

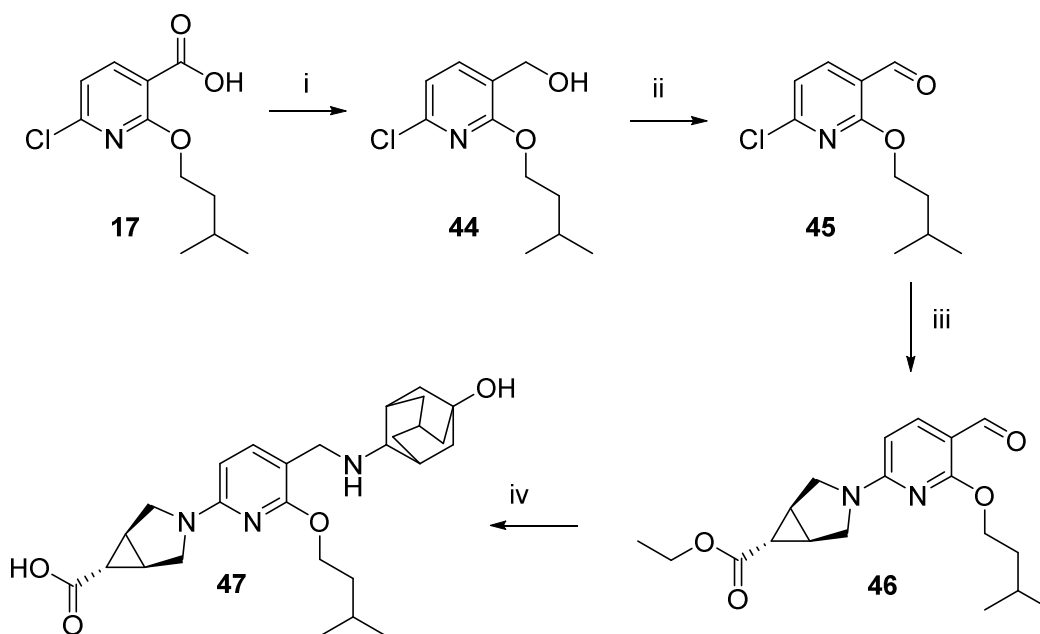


Reagents: i. Amine, DIPEA, THF/DCM 39%. ii. 3-methyl butanol, potassium t-butoxide, THF, 85%. iii. Amine, DIPEA, butyronitrile, 70%. iv. Aq NaOH in methanol, 18%.

Reaction of the commercially available 2,6-dichloropyridine-3-sulfonyl chloride with 4-aminoadamantan-1-ol to give **40** followed by sequential displacements of halogen by 3-methylbutoxide and ethyl (1R,5S,6R)-3-azabicyclo[3.1.0]hexane-6-carboxylate followed by hydrolysis to the carboxylic acid gave compound **43**.

The des-carbonyl compound **47** was prepared by the route shown in Scheme 5 below.

Scheme 5 Synthesis of 'des-carbonyl' compound 47.

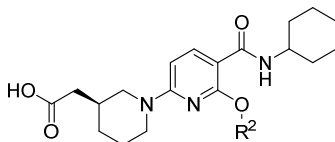


Reagents: i. Borane-tetrahydrofuran complex 1M in THF 80%. ii Dess-Martin periodinane, 15 wt.% in DCM, 65%. iii. Amine, DIPEA, butyronitrile, 80%. iv. a. 4-Amino-1-adamantanol, sodium borohydride, methanol. b. NaOH, aq. Methanol, 4%.

Compound **17** was reduced to alcohol **44** and then oxidised to give aldehyde **45** which was reacted with ethyl (1R,5S,6R)-3-azabicyclo[3.1.0]hexane-6-carboxylate followed by addition of the hydroxyadamantyl amine by reductive amination and then hydrolysis of the ester to the carboxylic acid to give compound **47**, albeit with poor recovery after preparative HPLC purification.

Results.

Region R2. Compounds **16a** - **16az** with differing substituents in the core pyridine 2-position, R2, were intended to explore the topology and the nature of the small lipophilic pocket identified in the crystal structure of compound **3**. These compounds were screened in the IDH1 (R132H) biochemical assay, the results of which are shown in Table 2.

Table 2: Biochemical screening data for R² aliphatic substituents.

	R ²	IC ₅₀ μM ^a (SD)		R ²	IC ₅₀ μM ^a (SD)
12		6.4 (1.9)	16m		16 (4.4)
16a		8.0 (0.95)	16n		26 (12.7)
16b		7.6 (2.4)	16o		14 (7.5)
16c		9.7 (4.4)	16p		20 (6.9)
16d		7.2 (3.2)	16q		30 (3.3)
16e		12 (2.1)	16r		20 (12.8)
16f		12 (2.7)	16s		>50
16g		12 (3.1)	16t		>50
16h		15 (0.47)	16u		>50
16i		12 (5.1)	16v		>50
16j		14 (2.7)	16w		>50
16k		14 (4.7)	16x		>50
16l		12 (5.9)	16y		>50

^aIC₅₀s are mean values of a minimum of 3 replicates. Standard deviations are listed in parentheses.

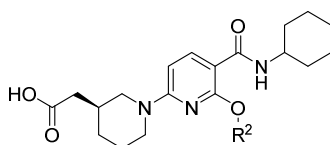
The introduction of a heteroatom (i.e. N or O) to the substituent was poorly tolerated, as exemplified by the methyl ether compound **16s**, pyranyl compound **16t** and dimethylamine compound **16w**, which were all inactive ($IC_{50} > 50 \mu M$). These results were consistent with the X-ray crystallographic data from the original hit, which showed that the alkyl group at the 2-position occupies a lipophilic pocket devoid of any potential polar interactions. Reducing the length of the O-linked alkyl chain at the 2-position to an isobutyl **16n**, ethyl **16u** or methyl group **16v** all led to a 3-fold to >7-fold drop off in potency. Given the potencies observed for similarly sized moieties at this position, these data (and the data for **16x** and **16y**) are rather surprising and remain unexplained.

Attempts to reduce the conformational flexibility of the 2-substituent by introducing sp^2 character or a small ring, compounds **16a**, **16d**, **16j**, **16p** and **16q**, all led to a decrease in the potency compared with compound **12**. The introduction of a 1,1,1-trifluorobutoxy group **16h** resulted in a 2-fold decrease in the activity towards IDH1 (R132H) compared with an isopentyl group, roughly equipotent with the butoxyl compound **16g**. All this provided confirmation that the binding pocket of the IDH1 (R132H) enzyme preferred lipophilic, non-polar groups at the 2-position of the pyridine ring and that from the examples prepared, the isopentyl moiety was optimal.

The introduction of a variety of different substituted O-linked benzyl groups at this position bearing electron-donating or electron-withdrawing substituents are shown in Table 3. Unsubstituted benzyl compound **16z** gave an IC_{50} of $8.6 \mu M$, representing a marginal decrease in the potency compared with the isopentyl group at this position, **12**.

The addition of an electron-donating methyl group to the phenyl ring of the benzyl group had a significant impact on the activity of these compounds. For example, the ortho-methyl, compound **16aa** and meta-substituted benzyl, compound **16ab**, compounds led to a two-fold increase in the potency compared with the unsubstituted system compound **9z**. However, the corresponding para-substituted compound **16ac** was inactive against IDH1 (R132H). Methoxy-substituted benzyl systems, however, gave a marginal loss in potency for ortho- and meta-substituted benzyl groups, compounds **16ad** and **16ae** while the para-methoxy substituted benzyl compound **16af** was inactive. Interestingly, **16ad** and **16ae** contrast strongly with **16s** and **16t**, where an oxygen atom in a similar spatial location is clearly not tolerated, perhaps highlighting a requirement for additional steric bulk or lipophilic interactions. The introduction of electron-withdrawing substituents onto the phenyl ring of the benzyl group was also investigated. In contrast to the results observed for the electron-donating substituents, the introduction of a fluoro or chloro substituent was tolerated in all positions of the phenyl ring showing only a marginal increase in potency for the ortho fluoro compound **16ag** and equivalent potency for fluorine in the m- and p-positions and chlorine in all positions.

Table 3. IDH1 (R132H) enzyme assay data for R2 substitutions.



	R	IC ₅₀ μM ^a (SD)		R	IC ₅₀ μM ^a (SD)
12		6.4 (1.9)	16ai		8.8 (3.6)
16z		8.6 (3.7)	16aj		7.0 (1.8)

	R	IC ₅₀ μM ^a (SD)		R	IC ₅₀ μM ^a (SD)
16aa		4.5 (1.3)	16ak		9.9 (11)
16ab		4.6 (0.08)	16al		7.7 (0.49)
16ac		>50	16am		43 (4.7)
16ad		13 (0.37)	16an		5.9 (0.87)
16ae		12 (0.65)	16ao		11 (1.1)
16af		>50	16ap		5.8 (1.0)
16ag		5.6 (0.32)	16aq		38 (7.1)
16ah		10 (3.1)			

^aIC₅₀s are mean values of a minimum of 3 replicates. Standard deviations are listed in parentheses.

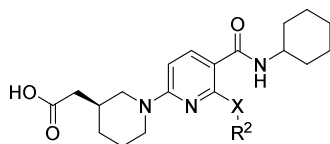
The introduction of a methyl group at the α-benzylic position of the unsubstituted benzyl was investigated, with the (R)-enantiomer, compound **16an**, showing a small increase in potency compared with the unsubstituted system; conversely the (S)-enantiomer, compound **16ao** showed

a small loss in potency. Extending from benzyl to phenethyl (**16am**) gave a significant decrease in the potency, consistent with the small size of the binding pocket.


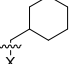
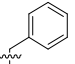
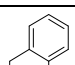
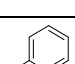
Taken together, these data show that the introduction of an ortho-methyl substituted benzyl system at the 2-position of the pyridine ring was the optimal benyl moiety, albeit delivering only a marginal increase in potency at best, compared with the isopentyl substituent (4.5 vs. 6.4 μM). Combination of the ortho-methyl group and an α -methyl group compound **16ap** showed no advantage over the individual substitutions whilst combination of the ortho-methyl group and a para-chloro group compounds **16aq** was detrimental.

In order to understand the influence of linkers other than oxygen on the SAR, a small set of matched pairs were prepared in a similar manner to that shown in Scheme 1, using the appropriate starting materials with O, N and S linker atoms. Full details of synthesis are given in the experimental section.

Table 4. IDH1 (R132H) enzyme assay data IC_{50} (μM) for R2 and X substitutions



X	O		S		N	
		$\text{IC}_{50} \mu\text{M}^a$ (SD)		$\text{IC}_{50} \mu\text{M}^a$ (SD)		$\text{IC}_{50} \mu\text{M}^a$ (SD)
	12	6.4 (1.9)	16ar	10 (1.3)	16av	>50

	16e	12 (2.1)			16aw	>50
	16c	9.7 (4.4)			16ax	>50
	16z	8.6 (3.7)	16as	39 (9.8)	16ay	>50
	16aa	4.5 (1.3)	16at	>50	16az	>50
	16ag	5.6 (0.32)	16au	21 (5.4)		

^aIC₅₀s are mean values of a minimum of 3 replicates. Standard deviations are listed in parentheses.

Comparison of the IDH1 (R132H) activities of the O-isopentyl compound **12** and S-isopentyl compound **16ar** showed only a small difference in potencies (Table 4). However, it was apparent that in all other examples that the S-linkage was inferior to O-linkage and that the N-linkage was not tolerated at all, perhaps as a result of the change from an H-bond acceptor to an H-bond donor.

Summarising SAR in this region, having investigated a wide variety of small lipophilic groups in the R2 position, -O-isopentyl and -O-ortho-methylbenzyl were found to be the preferred substituents for this vector.

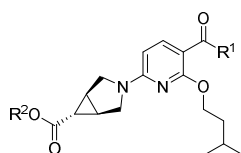
Region R1. Compounds **20a** – **20af** with differing substituents on the pyridine 3-carboxamide, R1, were intended to explore topology and the nature of the more open and less well defined pocket identified in the crystal structure of compound **9**. The results of the investigation can be

seen in Table 5, all new compounds were compared against the R1 cyclohexyl carboxamide compound **20ab**, enzyme IC₅₀ 7.9 μM.

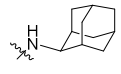
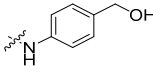
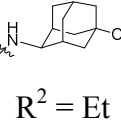
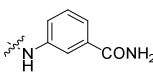
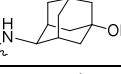
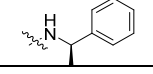
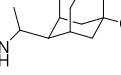
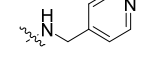
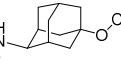
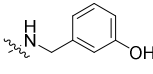
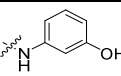
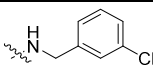
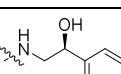
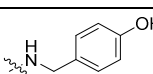
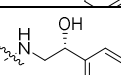
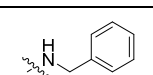
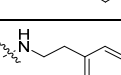
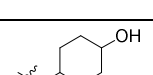
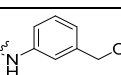
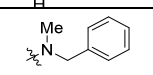
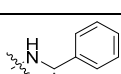
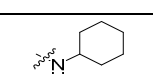
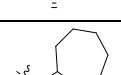
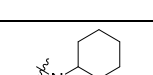
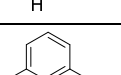
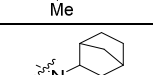
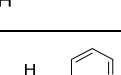
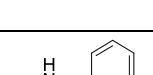
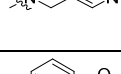
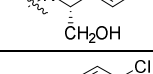
Aliphatic and cycloaliphatic groups, with or without the addition of hetero atoms or single bridge structures, failed to offer any increase in potency against IDH1 (R132H) except for **20l**. Direct aryl attachments gave a range of inhibitory activities from unsubstituted phenyl (>50 μM) (not shown in Table 5) to **20f** (2.9 μM), compounds with a hydroxyl pendent group (direct or indirect) being the most potent suggesting the possibility of a positive interaction between the hydroxyl group and the protein structure.

Benzyl carboxamides gave a range of activities. The baseline benzyl substituent group **20y** was marginally improved upon by simple monosubstitutions and modest (up to 2-fold) improvements were obtained from the R-α-methyl compound **20t** and the S-α-methyl compound **20k**. Extending the aryl group further with R1 as phenethyl, **20i**, gave an additional small increase in enzyme potency.

Table 5. IDH1 (R132H) enzyme assay data (μM) for R1 substitutions.



	R1	IC ₅₀ μM ^a (SD)		R1	IC ₅₀ μM ^a (SD)
12		6.4 (1.9)	20p		5.0 (0.74)
20a		0.27 (0.22)	20q		12 (13)

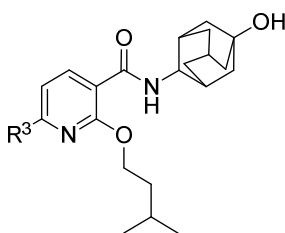
20b		>50	20r		5.6 (0.95)
19a	 R ² = Et	13.5 (11)	20s		6.0 (0.94)
20c		0.27 (0.14)	20t		5.4 (1.9)
20d		0.23 (0.02)	20u		6.2 (1.1)
20e		0.86 (0.33)	20v		6.3 (1.3)
20f		2.9 (0.09)	20w		6.5 (2.0)
20g		3.1 (0.44)	20x		6.6 (1.8)
20h		3.0 (0.46)	20y		9.4 (1.6)
20i		3.9 (0.70)	20z		8.2 (2.2)
20j		3.2 (0.67)	20aa		7.4 (3.4)
20k		4.4 (0.51)	20ab		7.9 (3.5)
20l		3.9 (0.69)	20ac		17 (4.5)
20m		4.6 (0.54)	20ad		14 (8.6)
20n		5.6 (1.7)	20ae		5.6 (0.95)
20o		5.4 (0.26)	20af		17 (11)

^aIC₅₀s are mean values of a minimum of 3 replicates. Standard deviations are listed in parentheses. R²=H in all cases except where stated otherwise (20??)

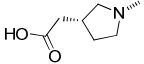
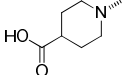
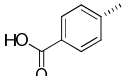
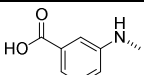
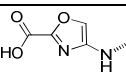
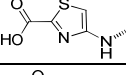
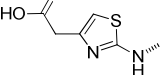
The most significant improvements in IDH1 (R132H) inhibition came from the use of bulkier structures. Although the adamantyl carboxamide **20b** was essentially inactive ($>50 \mu\text{M}$), substitution of the adamantyl group in the 1-position with hydroxyl **20a** or methoxy **20c** gave compounds with sub-micromolar activity. Extending the hydroxyadamantyl group further from the carboxamide link with a methyl substituted methylene **20d** gave a similar sub-micromolar level of activity whilst the addition of a difluoromethoxy group **20e** gave a noticeable decrease in activity, albeit still at a submicromolar level.

Region R3. Simple replacement of the carboxylic acid group of **20b** by ethyl ester (**19a**) dramatically reduced activity, as might be expected by elimination of the key interaction with Arg119. Although a number of alternative carboxylic acid scaffolds were tolerated, it was noted that the scaffolds in **20b**, **21** and **22** were the most effective (Table 6). One exception to this trend was the thiazole carboxylic acid **26** which displayed submicromolar potency, although this is still some three- fold less active than the most potent compound **20a**.

Table 6. IDH1 (R132H) enzyme assay data (μM) for R3 substitutions.



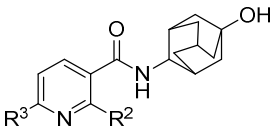
	R ³	IC ₅₀ μM^a (SD)
20a		0.27 (0.22)
21		1.3 (0.33)

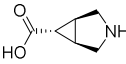
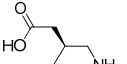
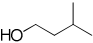
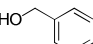
22		1.2 (1.3)
23		3.4 (1.1)
24		3.0 (6.5)
25		11 (2.4)
26		21 (6.7)
27		0.81 (0.32)
28		>50

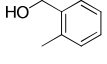
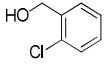
^aIC₅₀s are mean values of a minimum of 3 replicates. Standard deviations are listed in parentheses.

With this information to hand, a set of compounds were then synthesized combining the more potent R2 and R3 components with the hydroxyadamantyl carboxamide R1 group to examine the additive nature of the group SAR.

Table 7. Matched pair combinations of R2 and R3 substitutions, IDH1 R132H IC₅₀ μM.



R3		
	IC₅₀ μM^a (SD)	IC₅₀ μM^a (SD)
	20a 0.27 (0.22)	21 1.2 (0.33)
	29 27 (15)	32 2.3 (0.79)

	30 4.5 (4.7)	33 0.69 (0.30)
	31 3.2 (2.0)	34 2.3 (0.39)

^aIC₅₀s are mean values of a minimum of 3 replicates. Standard deviations are listed in parentheses.

It is evident from the results in Table 7 that the component SAR is not truly additive and that the overall SAR is dominated by the R3 carboxylic acid group. It is logical to suggest that the rigid nature of the aza-bicyclohexane acid, which gave rise to the most potent inhibitors with a small subset of R1 and R2 groups, would be less tolerant of alternative R2 substitutions than the more flexible (and accommodating) piperidine acetic acid.

The X-ray crystal structure obtained for compound **9** indicated that there may be some potential for hydrogen bonding between the pyridine carboxamide -NH- with Tyr285 and -CO- with His132, in this latter case via water mediation. In order to understand further the importance of the role of the 3-carboxamido group, compounds were prepared modifying the nature of the 3-carboxamide group by substitution, by reversal of the carboxamide or by replacement with other groups.

A comparison of benzyl carboxamide compound **20y** and cyclohexyl carboxamide compound **20ab** with the N-methyl analogues, **20aa** and **20ac** shows either no change or a small loss of potency on replacement of the carboxamide -NH- by -NMe-, suggesting that either any potential internal hydrogen bond to the pyridyl 2-oxygen atom added little to the potency of the compounds or the increased rotational freedom of the amide bond is beneficial.

Replacement of the pyridine carboxamide with the reversed carboxamide, **39a** or urea **39b** resulted in complete loss of activity, as did direct replacement of the carbonyl group with a sulfonamide **43** (Figure 6). Further, reduction of the carbonyl group completely to yield **47**, resulted in a complete loss of activity suggesting that the carbonyl group has a role in hydrogen bonding and/or rotational stability. Only the reverse sulfonamide **39c** (8.6 μ M) was found to have a similar potency when compared to **20ab**. Here, perhaps, the differing geometry allows a strong hydrogen bond with His132 or reorientates the R1 lipophilic group improving contact with the enzyme, presenting an opportunity for further study.

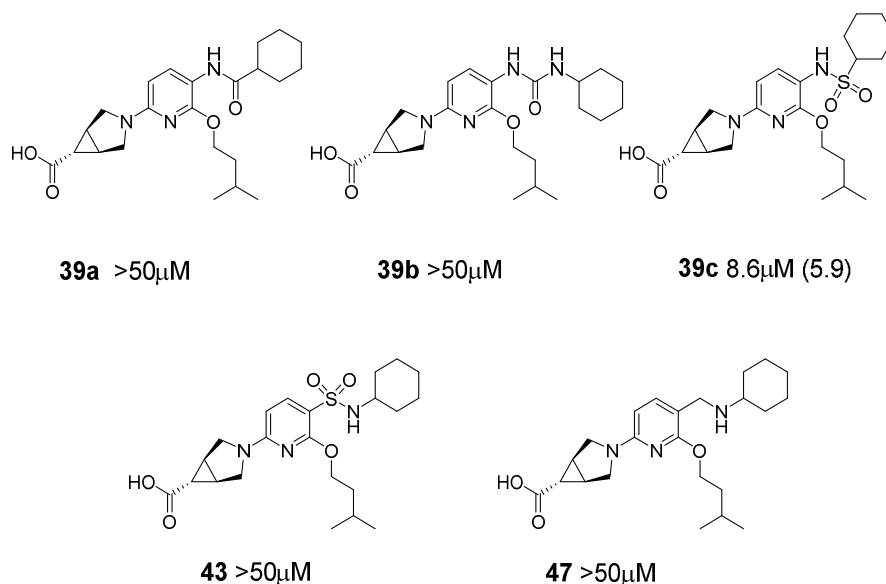


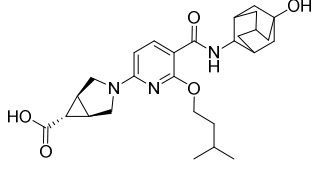
Figure 6. IDH1 IC₅₀ results for carboxamide replacements. ^aIC₅₀s are mean values of a minimum of 3 replicates. Standard deviations are listed in parentheses.

Having established that compound **20a** was a potent compound against IDH1 (R132H) in this series we chose to re-examine selectivity against other related enzymes (Table 8).

Whilst retaining some activity against an alternative mutant IDH1 (R132C), (0.47 μ M), compound **20a** was inactive against both wild type IDH1 and IDH2 and glucose-6-phosphate

dehydrogenase (G6PD). There remained, however, a considerable potency against the original (AZ) target for this series of compounds, 11- β HSD-1, at 0.009 μ M.

Table 8. Selectivity of compound **20a** against related enzymes

	 20a					
	IDH1 R132H	IDH1 R132C	IDH1 wt	IDH2 wt	G6PD	11- β HSD1
IC ₅₀ /I C ₅₀ μ M ^a	0.27 (0.22)	0.47 (0.03)	>50	>50	>50	0.009

^aIC₅₀/IC₅₀s are mean values of a minimum of 2 replicates. Standard deviations are listed in parentheses.

Selected compounds with a range of enzyme inhibitions (including a related but inactive analogue **16v**) were screened in a cellular assay (using mutated R132H isocitrate dehydrogenase 1 transfected HEK293T cells – see Experimental section) measuring the inhibition of production of 2-HG directly by mass spectrometry (Table 9).

Table 9. Enzyme and cell activities (IC₅₀ μ M) for a selected set of compounds

Cmpd	Structure	Enzyme IC ₅₀ μ M ^a (SD)	Cell IDH1 IC ₅₀ μ M ^{a,b} (SD)	Hela cytotox μ M ^{a,c}
------	-----------	--	---	--

^aIC₅₀s are mean values of a minimum of 2 replicates. Standard deviations are listed in parentheses. ^bIC₅₀ Inhibition of production of 2-HG measured directly by mass spectrometry. ^cIC₅₀ Proliferation assay in non-IDH driven cell line

Structure of compound **20a** complex with IDH1 (R132H).

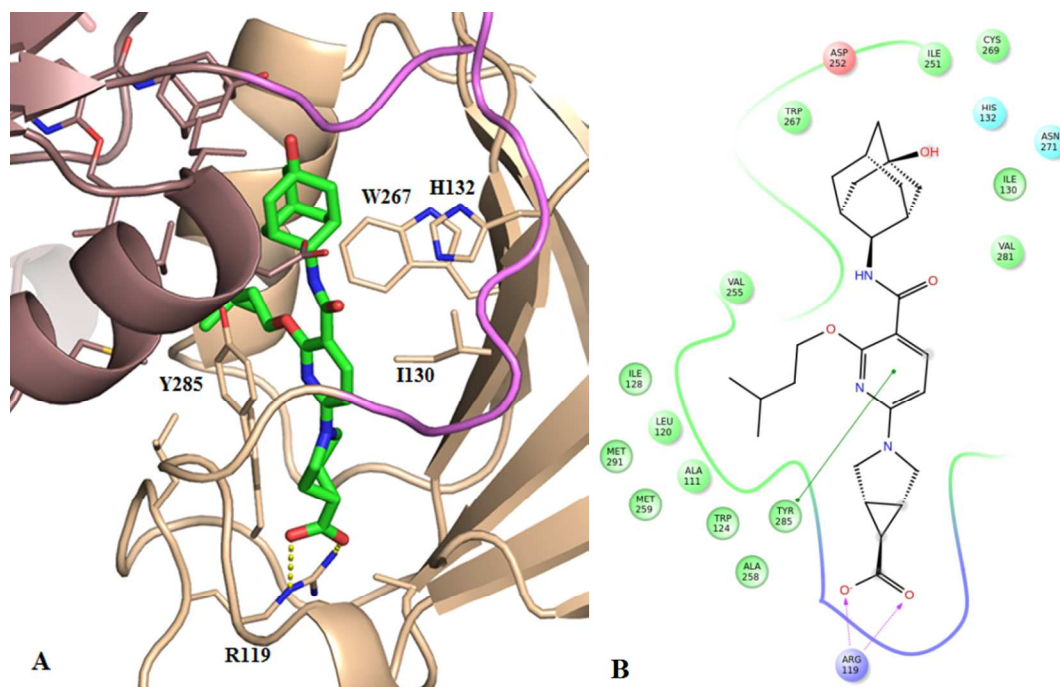


Figure 7. (A) Crystal structure of compound **20a** in IDH1 (R132H). PDB accession code 5L57, previously unresolved loops highlighted in magenta (B) Protein:ligand interaction diagram

A series of surface entropy reduction mutations were made to R132H to enhance the repeatability of the crystallogenes. In all five additional surface residues were mutated (E80A, K81A, E240A, Q242A & K243A) to alanine residues. These mutations produced a construct R132H* that behaved favourably during crystallogenes and was subsequently used throughout this study.

The crystal structure of compound **20a** complexed with IDH1 (R132H) homodimer in the presence of NADPH (PDB accession code 5L57) was obtained at 2.7 Å (Figure 7). Electron density for compound **20a** and for cofactor was found in both dimer subunits.

This crystal structure is very similar to that obtained with compound **9**, with the inhibitor binding at the interface of the two components of the protein dimer. The ionic interaction between the carboxylic acid of compound **20a** and Arg119 is unchanged from the crystal structure of

compound **9**, as is the pi-stacking of the central pyridine ring with the side chain of Tyr285. The pyridyl 2-isopentoxide group occupies the same lipophilic pocket bounded by the residues Leu120, Val121, Trp124, Val255 and Met259 but perhaps makes better contacts. There is an internal hydrogen bond between the -NH- of the pyridine 3-carboxamide and 2-O linker, but no hydrogen bond with the oxygen atom of Tyr 285. The 3-carboxamide carbonyl group points in the general direction of His132 but is again too distant for direct hydrogen bonding. The pendant hydroxy adamantyl group is situated in the same area as in the structure of compound **9**, making several lipophilic contacts but no direct hydrogen bonds from the hydroxyl group. Note that, as in the previous structure, solvent molecules were not resolvable at this resolution.

In this crystal structure there is sufficient electron density to assign several previously missing loops including Tyr272-Val281 and Lys212-Lys218. Of these newly resolved residues, only Val281 interacts directly with the ligand, providing an additional lipophilic contact with the pyridyl ring.

It is informative to compare this crystal structure with those of previously published allosteric inhibitors **3** and **6** (Figure 8). The binding mode of **20a** can be summarized in terms of four key pharmacophore features: hydrogen-bonding between the acidic moiety and Arg119; aromatic stacking between the pyridyl and Tyr285; lipophilic contacts between the isopentyl moiety and the enclosed dimeric pocket around Val255 and Met 259; and looser lipophilic contacts around the adamantyl moiety. Of these interactions, only lipophilic filling of the Val255/Met259 pocket is a consistent feature. In the Sanofi Bisimidazole **3**²⁰ structure, this pocket is enlarged due to Trp267 adopting an alternative rotamer, allowing a bulky branched octyl moiety to be accommodated. Overall, the ligand occupies a similar binding location to **20a**: when the binding

1
2
3 sites are overlaid, the central phenol is observed to be somewhat displaced from the pyridyl of
4
5 **20a**, with the two imidazole moieties aligning loosely with the adamantyl and aza-bicyclohexane
6
7 moieties of **20a**. A notable difference between the structures is the significant re-positioning of
8
9 the Asn271-Gly286 loop, with Ser280-Gly284 now adopting a short helical structure. As a result,
10
11 Tyr285 is significantly displaced and hence not available to pi-stack to the phenol ring; instead,
12
13 the sidechain of Val281 now occupies a similar position. A further consequence is that Asp279
14
15 moves closer to the ligand and forms a direct hydrogen bond with the phenolic hydroxyl. The
16
17 sidechain of Arg119, which formed an ion pair with the acidic moiety of **20a**, adopts a different
18
19 rotamer and does not interact with **3**.

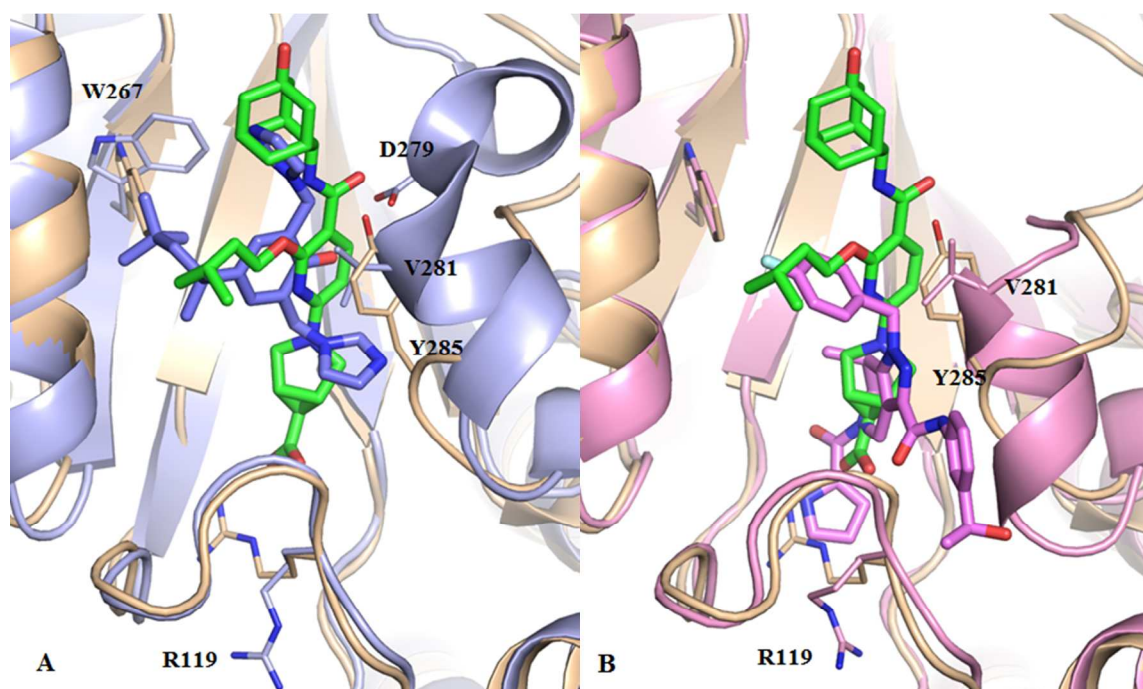


Figure 8. Comparison of inhibitor binding modes in crystal structures of **20a** (green ribbons and carbon atoms) with (A) **3** (PDB 4UMX) and (B) **6** (PDB 5DE1). For clarity, only chain A and selected residues shown.

Inhibitor **6** again binds in the dimer interface but displays some strikingly different interactions.

Although Ser280-Gly284 forms a short helix similar to that in the Sanofi structure, most of this

loop (Asn271-Asp279) is unresolved. The pyrazolopiperidine ring system of **6** overlays with the aza-bicyclohexane of **20a**, with the fluorobenzyl moiety of **6** filling the Val255/Met259 lipophilic pocket. The pyrrole ring of **6** extends beyond the acidic moiety of **20a**, in effect displacing the sidechain of Arg119. However the most notable difference is the location of the hydroxyethylanilino substituent, which extends between the Ser280-Gly284 helix and the Ile112-Pro127 loop into a region not occupied by either **3** or **20a**. Direct protein:ligand hydrogen bonds, unique to **6**, are formed between the carboxamide linker and the backbone atoms of Leu120 and Val281, and between the pyrrolo carbonyl and Ile128.

Recently, the binding mode of the Agios allosteric inhibitor 2-(2-(1H-benzo[d]imidazol-1-yl)-N-(3-fluorophenyl)acetamido)-N-cyclopentyl-2-o-tolylacetamide (ML309) has been established by cryoelectron microscopy²⁷. Although the resolution is too low to allow accurate placement of the inhibitor, it is evident that the compound is occupying a binding site at the dimer interface which is broadly similar to that seen for the above compounds.

Although the structural basis of inhibitor selectivity for mutant over wild type IDH1 is not fully understood, it is apparent that these inhibitors bind to a conformation of the protein in which the location of several catalytically important residues is significantly disrupted, including, for example, His132 and Tyr139 (involved in substrate binding) and Asp275 and Asp279 (involved in binding the catalytic magnesium ion). Hence, it is likely that allosteric inhibitors bind preferentially to an inactive conformation that is more accessible to the mutant protein than to wildtype. For example, Deng et al²⁰ highlight differences in binding affinity for the catalytic magnesium ion between mutant and wildtype IDH1. In summary, comparison of our crystal structures with those of other allosteric inhibitors reveals that the allosteric binding site is

accessible to lipophilic ligands of diverse chemotypes, which share some common binding interactions, notably to the Val255/Met259 lipophilic pocket, but also achieve a number of unique polar and lipophilic interactions. The allosteric binding site displays varying degrees of induced fit, as well as differences in the overall packing of the dimers, to accommodate these diverse ligands. Taken together, the crystal structures may guide the future optimization of allosteric inhibitors and facilitate the identification of additional allosteric chemotypes through focused screening campaigns.

We next tested compound **20a** in acute myeloid leukemia (AML) cells. Approximately 10% of patients carry IDH1 mutations and inhibitors of mutant IDH1 and IDH2 are currently being evaluated in early phase trials²⁸⁻³⁰. As no immortalized human AML cell lines carrying native IDH1 mutations are available, we generated an AML cell line system using THP1 AML cells, whereby Myc-tagged IDH1 R132H could be inducibly expressed following the addition of doxycycline (Figure 7A). As expected, induced expression of mutant IDH1 resulted in production of 2-hydroxyglutarate, and this was inhibited in a dose-dependent manner by compound **20a**, with IC₅₀ 1.9μM and complete reduction to baseline levels at ≥10μM. Interestingly, treatment of cells with compound **20a** had no effect on proliferation or differentiation (data not shown) suggesting limited off-target or non-specific cellular toxicity.

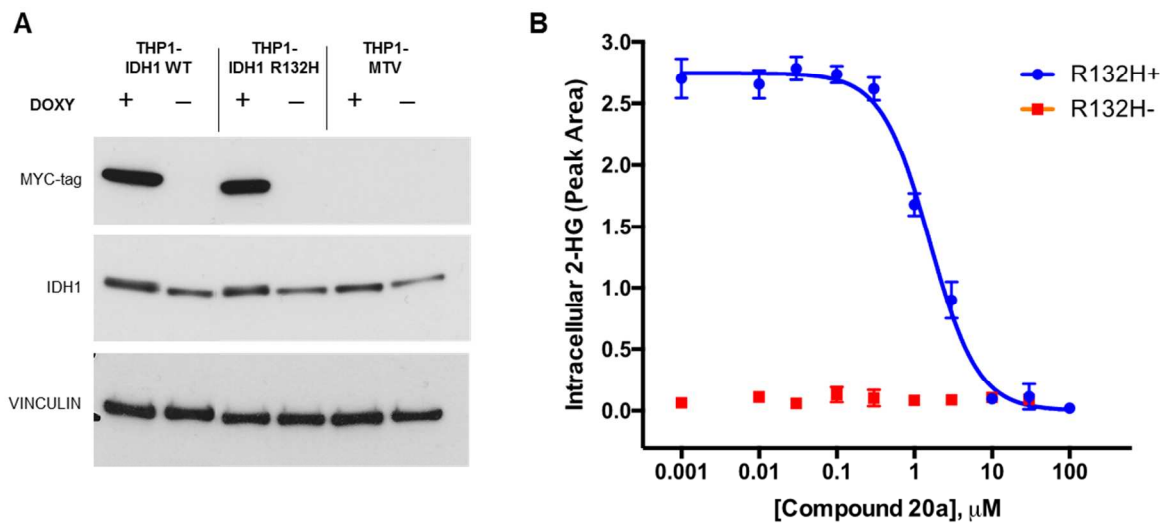


Figure 9. Isogenic AML cell line model of IDH1 R132H. THP1 AML cells were engineered to inducibly express wild type IDH1 or R132H mutant IDH1 under control of doxycycline (1 $\mu\text{g}/\text{ml}$). (A) Western blots show expression of the indicated proteins/epitopes in the indicated conditions. WT: wild type; MTV: empty vector; DOXY: doxycycline. (B) Dose-response curve for inhibition of 2-HG production by THP1-IDH1 R132H cells cultured for 5 days with (R132H+; blue line) or without (R132H-; red line) doxycycline and at the indicated doses of Compound **20a**.

We next tested the activity of compound **20a** versus primary AML blast cells (cultured in semisolid medium) from three IDH1 R132H-mutated patients (BB171; BB340; BB539; BB= Biobank number) and four IDH1 wild-type patients. Three doses of **20a** reflecting the cellular IC_{50} , $4\times\text{IC}_{50}$ and $8\times\text{IC}_{50}$, or DMSO vehicle control, were used. After 14 days in culture primary cells exposed to doses commensurate with near-total (9.2 μM) or total (18.4 μM) 2-HG reduction in THP1 cells exhibited significant myeloid differentiation compared with vehicle-treated controls, as evidenced by upregulation of the myeloid differentiation markers CD11b and CD15, downregulation of the stem cell marker CD117 (Figure 10A), and induction of mature cellular morphology (Figure 10B). Interestingly, treatment of IDH1 R132H-mutant primary AML cells with **20a** led to an increase in clonogenic activity (Figure 10D). This “proliferative burst” is associated with release of the differentiation block and has previously been described following

1
2
3 treatment of IDH2 mutant primary AML cells with the mutant IDH2 inhibitor AGI-67801²⁸. By
4
5 contrast, and in keeping with **20a** being selective for mutant IDH1, no differences in clonogenic
6
7 potential or myeloid differentiation were observed in similarly treated IDH1 wild type AML
8
9 blasts (Figure 10A, 10D).
10
11
12
13
14
15
16
17
18
19
20
21
22
23
24
25
26
27
28
29
30
31
32
33
34
35
36
37
38
39
40
41
42
43
44
45
46
47
48
49
50
51
52
53
54
55
56
57
58
59
60

Figure 10

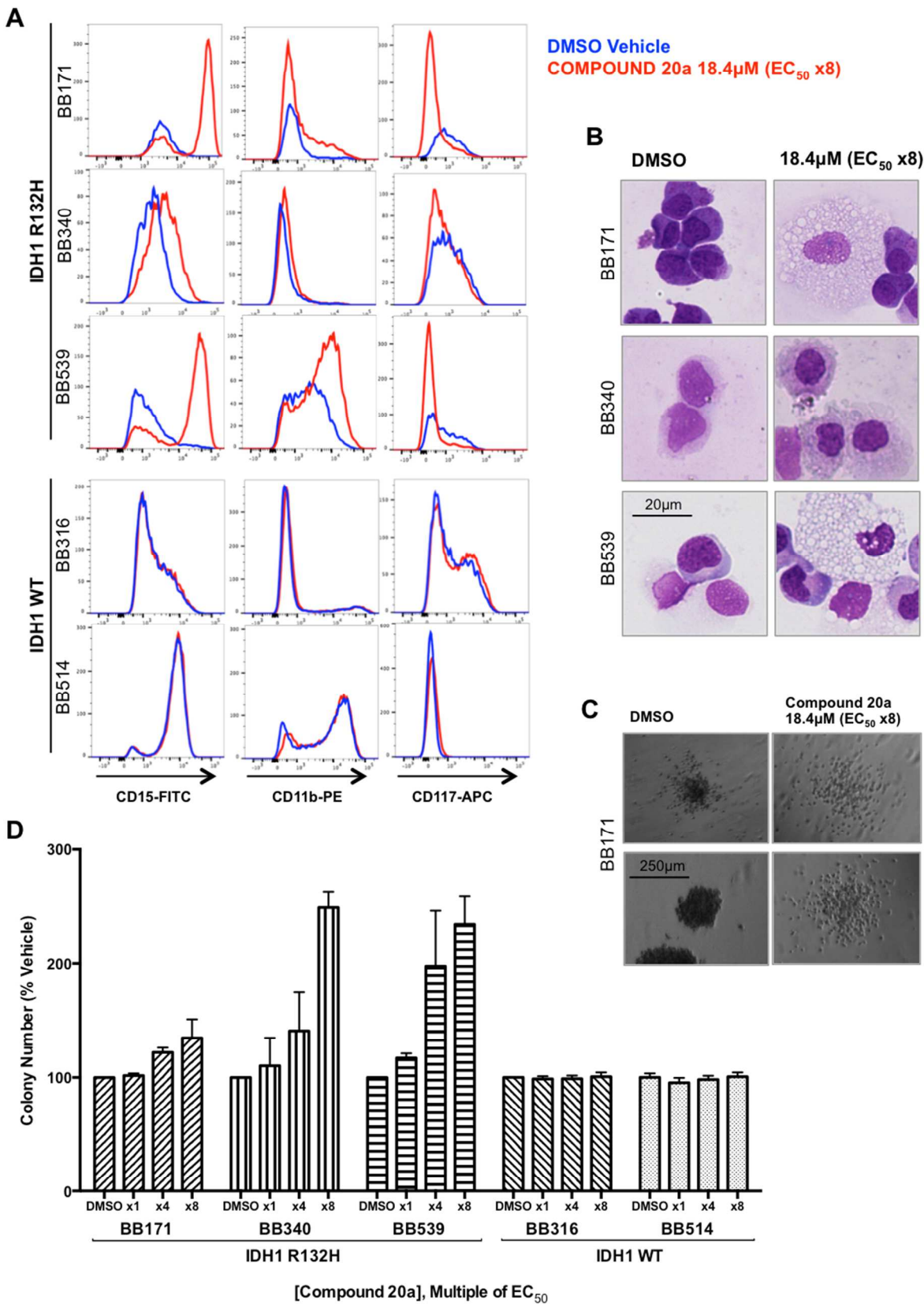


Figure 10. Compound 20a induces myeloid differentiation in primary human IDH1 R132H AML cells *ex vivo*. (A) Flow cytometry histograms for CD11b, CD15 and CD117, (B) cytospin preparations, (C) indicative colony morphologies and (D) total colony numbers relative to vehicle-treated control cells from the indicated patients after 14 days *ex vivo* methylcellulose culture with Compound **20a** 18.4 μ M (red) or DMSO vehicle (blue). Error bars represent mean \pm standard error of three independent experiments.

Conclusions

As part of a collaborative program, a high throughput screen of 1.35 million compounds against isocitrate dehydrogenase IDH1 (R132H) led to the identification of three series of inhibitors, which when resynthesized, reduced to a single series (having discarded several positives potentially arising as a result of assay interference by metal contamination). The remaining hit series was rapidly optimized to a moderately potent, cell active compound.

Elucidation of the crystal structure of **9** showed that this series of inhibitors exhibited a novel binding mode in a previously identified allosteric site of IDH1 (R132H). Subsequent elucidation of the crystal structure of the complex between IDH1 (R132H) and inhibitor **20a** allowed the position of the previously unresolved protein loop to be observed and it is hoped that this more complete structure will aid the design of future inhibitors of IDH1 (R132H).

When tested using in vitro assays, the most encouraging compound, **20a** promoted differentiation of patient derived human IDH1 R132H AML cells, but not in IDH1 wild type AML cells, confirming on-target activity in a primary cell setting.

Experimental

Chemical Experimental.

All reagents obtained from commercial sources were used without further purification.

Anhydrous solvents were obtained from the Sigma-Aldrich Chemical Co. Ltd. or Fisher Chemicals Ltd. and used without further drying. Solutions containing products were either passed through a hydrophobic frit or dried over anhydrous MgSO_4 or Na_2SO_4 , and filtered prior to evaporation of the solvent under reduced pressure. Thin layer chromatography (TLC) was conducted with 5 cm \times 10 cm plates coated with Merck type 60 F254 silica gel to a thickness of 0.25 mm. Chromatography was performed on Biotage SNAP HP-Sil cartridges using a CombiFlash Companion machine. Proton (^1H) NMR spectra were recorded on a 300 MHz Bruker spectrometer at ambient temperature. Solutions were typically prepared in either deuteriochloroform (CDCl_3) or deuterated dimethylsulfoxide (DMSO-d_6) with chemical shifts referenced to deuterated solvent as an internal standard. ^1H NMR data are reported indicating the chemical shift (δ), the multiplicity (s, singlet; d, doublet; t, triplet; q, quartet; m, multiplet; br, broad; dd, doublet of doublets, etc.), the coupling constant (J) in Hz and the integration (e.g. 1H). Deuterated solvents were obtained from the Sigma-Aldrich Chemical Co., Goss or Fluorochem. LCMS spectra with UV detection were recorded on a Waters Acquity UPLC. Mass spectrometry was performed on a Waters Acquity SQD quadrupole spectrometer running in dual ES^+ and ES^- mode. High pH runs were conducted at pH 10 and low pH runs were conducted at pH 4, with a run time of 2 min. The column temperature was 40 $^\circ\text{C}$, and the flow rate was 0.6 mL/min. Further details, including solvent gradients, are given in the Supporting Information. Details of the

preparative HPLC instrument and the solvent gradient used to purify compounds are also given in the Supporting Information. All compounds were 95% purity as determined by examination of both the LCMS and ^1H NMR spectra unless otherwise indicated. When Cl or Br was present, expected isotopic distribution patterns were observed.

Preparation of Compound **20a**.

6-Chloro-2-(isopentyloxy)-3-pyridine carboxylic acid (17)

3-Methylbutan-1-ol (9.93 mL, 91.2 mmol) was added to a stirred suspension of sodium hydride, (60% dispersion in mineral oil) (4.17 g, 104.2 mmol) in a mixture of DCM (200 mL) and THF (100 mL) at 0 °C. After 20 minutes of stirring, 2,6-dichloropyridine-3-carboxylic acid (5. g, 26.0 mmol) was added portion wise over 10 minutes and the resultant mixture allowed to stir at room temperature for 96 hours. To the mixture was added water (300 mL) and the aqueous layer was collected. The DCM was solution was extracted once more with water (150 mL) and the combined aqueous layers were then acidified to pH 1 using conc. HCl. The acidic aqueous was then extracted with DCM 3 x (150 mL) and EtOAc (100 mL). The combined organic solution was dried over MgSO_4 and concentrated *in vacuo* to afford residue that was purified on a 100g SNAP column using a 0-5% MeOH:DCM eluent to afford 6-chloro-2-isopentyloxy-pyridine-3-carboxylic acid **17** (4.69 g, 19.2 mmol, 73.9%) as a white solid. ^1H NMR (300 MHz, CDCl_3) δ 9.62-11.28 (m, 1H), 8.37 (d, $J=8.01$ Hz, 1H), 4.61 (t, $J=6.55$ Hz, 2H), 1.76 (br dd, $J=3.96$, 6.22 Hz, 3H), 0.98 (br d, $J=6.31$ Hz, 6H) High pH RT = 0.77 mins, $[\text{M}-\text{H}]^- = 242.1$.

6-((1R,5S,6R)-6-(Ethoxycarbonyl)-3-azabicyclo[3.1.0]hexan-3-yl)-2-(isopentyloxy)-3pyridine carboxylic acid (18)

To a stirred solution of 6-chloro-2-isopentyloxy-pyridine-3-carboxylic acid **17** (2.52 g, 10.35 mmol) in butyronitrile (25 mL) was added N,N-diisopropylethylamine (5.13 mL, 31.1 mmol) followed by ethyl 3-azabicyclo[3.1.0]hexane-6-carboxylate (1.65 mL, 10.9 mmol) and the resultant mixture stirred at 100 °C for 96 hours. The mixture was then concentrated *in vacuo* and purified directly on a 24g SNAP cartridge using EtOAc:isohexane 0-100% as eluent to afford 6-[(1S,5R)-6-ethoxycarbonyl-3-azabicyclo[3.1.0]hexan-3-yl]-2-isopentyloxy-pyridine-3-carboxylic acid **18** (2.37 g, 6.54 mmol, 63%) as a golden oil that solidified on standing to an orange solid. ¹H NMR (300 MHz, CDCl₃) δ 9.94-10.72 (m, 1H), 8.07 (d, J=8.57 Hz, 1H), 5.95 (d, J=8.67 Hz, 1H), 4.47 (t, J=6.64 Hz, 2H), 4.08 (d, J=7.16 Hz, 2H), 3.67-3.96 (m, 2H), 3.56 (br s, 2H), 2.22 (br s, 2H), 1.67 (s, 3H), 1.49 (s, 1H), 1.20 (t, J=7.11 Hz, 3H), 0.91 (d, J=6.22 Hz, 6H) High pH RT = 0.93 mins, [M-H]⁻ = 361.2.

(1R,5S,6R)-3-(5-((5-Hydroxyadamantan-2-yl)carbamoyl)-6-(isopentyloxy)pyridin-2-yl)-3-azabicyclo[3.1.0]hexane-6-carboxylic acid (20a)

HATU (40.4 mg, 0.11 mmol) was added to a stirred solution of 6-[(1S,5R)-6-ethoxycarbonyl-3-azabicyclo[3.1.0]hexan-3-yl]-2-isopentyloxy-pyridine-3-carboxylic acid **18** (35. mg, 0.10 mmol) and triethylamine (40 µL, 0.29 mmol) in DMF (2 mL) and the resulting mixture was stirred for 30 minutes at room temperature. 4-aminoadamantan-1-ol (0.10 mmol) was then added and the mixture stirred for 2 hours. The reaction mixture was partitioned between EtOAc (10 mL) and water (10 mL). The organic layer was collected and the aqueous solution extracted with a further portion of EtOAc (10 mL). The combined organic solvents were washed with water (10 mL) and brine (10 mL), dried over Na₂SO₄ and concentrated to an oil. The crude intermediate was dissolved in 1,4-dioxane (2 mL) and a solution of sodium hydroxide (77.3 mg, 1.93 mmol) in

water (4 mL) was added and the mixture was stirred for 2 hours at 50 °C before being acidified to pH 1 with 2N HCl. The aqueous mixture was then extracted with EtOAc (2 x 50 mL) and the combined organic solution dried over MgSO₄ and concentrated *in vacuo*. The residue was purified by preparative HPLC (Low pH) to afford **20a**. ¹H NMR (300 MHz, DMSO-d₆) δ 8.02 (d, J=8.49 Hz, 1H), 7.91-8.00 (m, 1H), 6.11 (d, J=8.57 Hz, 1H), 4.31-4.64 (m, 3H), 3.99 (br s, 1H), 3.77 (br d, J=10.83 Hz, 2H), 3.51 (br d, J=11.49 Hz, 2H), 2.15 (br s, 2H), 1.89-2.09 (m, 3H), 1.57-1.85 (m, 11H), 1.46 (br d, J=12.43 Hz, 2H), 1.22-1.40 (m, 1H), 0.93 (d, J=6.31 Hz, 6H). ¹³C NMR (75 MHz, DMSO-d₆) δ 173.3, 162.7, 159.5, 156.7, 141.8, 102.4, 99.4, 65.4, 64.2, 52.0, 48.6, 44.3, 37.4, 33.5, 30.5, 25.5, 24.5, 22.2. HRMS [M+H]⁺ Found 484.2812. C₂₇H₃₈N₃O₅ requires 484.2811.

Biochemical assays.

All proteins used in the biochemical assays were produced by the Protein Expression Facility at the Manchester Institute of Biotechnology. The activity of the various dehydrogenase enzymes was measured by coupling NADPH consumption/production to a diaphorase/resazurin-based AmpliteTM detection system, measuring resorufin production.

All assays were performed in 384-well black plates (Corning #3575) in a reaction volume of 25 μL. IDH1 R132H was incubated at a final concentration of 32 nM with compounds in the presence of 20 mM Tris pH 7.5, 10 mM MgCl₂, 150 mM NaCl, 0.03 % BSA (w/v) buffer and 1mM α-ketoglutarate and 50 μM NADPH substrates. IDH1 R132C was incubated at a final concentration of 100 nM with compounds in the presence of 20 mM Tris pH 7.5, 10 mM MgCl₂, 150 mM NaCl, 0.03 % BSA (w/v) buffer with 0.5 mM α-ketoglutarate and 50 μM NADPH

substrates. IDH1 was incubated at a final concentration of 3 nM with compounds in the presence of 20 mM Tris pH 7.5, 1 mM MgCl₂, 150 mM NaCl, 0.03 % BSA (w/v) buffer with 0.2 mM isocitrate and 50 μM NADP substrates. IDH2 was incubated at a final concentration of 9 nM with compounds in the presence of 20 mM Tris pH 8.0, 1 mM MgCl₂, 150 mM NaCl, 0.03 % BSA (w/v) buffer with 0.2 mM isocitrate and 50 μM NADP substrates. G6PD was incubated at a final concentration of 7 nM with compounds in the presence of 20 mM Tris pH 8.0, 10 mM MgCl₂, 0.03 % BSA (w/v) buffer with 0.5 mM glucose-6-phosphate and 50 μM NADP substrates.

All reactions were initiated by the addition of NADPH/NADP. The assays were allowed to proceed at 26 °C for 30 mins (IDH1 R132C, IDH1 and G6PD) or 60 mins (IDH1 R132H and IDH2) before terminating with the addition of 5 μL Amplite™ detection system (The G6PD assay was stopped using 2.5 μL 0.5% SDS (w/v) prior to the addition of Amplite™). Following incubation at room temperature for 30 mins, fluorescence signal at Ex544/Em590 nm was measured using the BioTek Synergy 2 multi-mode plate reader.

11 β -HSD1 biochemical assay

11 β -Hydroxysteroid dehydrogenase (11β-HSD1) activity was measured in a coupled HTRF immuno-competitive assay. The assay was performed in 384-well black plates (Corning #3575) in a reaction volume of 10 μL in a buffer of 100 mM potassium phosphate pH 7.6 supplemented with 160 nM cortisone (Sigma # C2755), 1.5 μg / ml 11β-HSD1 (Cayman Chem # 10007815), test inhibitor compound, 1mM EDTA, 1 mM glucose-6-phosphate, 12.5 μg / ml glucose-6-phosphate dehydrogenase and, to start the reaction, 0.1 mM NADPH. The assay was allowed to

proceed at 37 °C for 30 mins before terminating with the addition of 5 μ L of 0.5 mM 11 β -glycyrrhetic acid (Sigma # G10105) prepared in cortisol-d2 solution (Cisbio # 7TRF30D). Following addition of the inhibitor / acceptor solution the assay signal was developed by the addition of 5 μ l of the donor antibody α -cortisol-cryptate (Cisbio # 7TRF30C). The plate was then incubated at room temperature for 2 hours before measuring the TR-FRET signal on a Pherastar FS Microplate Reader.

mutIDH1 R132H Cellular Mode of action Assay

20 μ l of Lipofectamine 2000 (Thermofisher #11668019) is added to 980 μ l of OptiMEM reduced serum media (Thermofisher #31985062). Separately 16 μ g of pcDNA3.1 mammalian expression vector (Thermo scientific #V79020) carrying isocitrate dehydrogenase 1 mutated at R132H was added to 1000 μ l of OptiMEM reduced serum media. Following 5 minutes incubation the solutions are mixed and incubated for 30 minutes at RT generating a transfection mix. Meanwhile HEK293T cells cultured in assay media (DMEM (Sigma #D6546), 10%FBS (Sigma #F7524), 2mM L-glutamine (Sigma #G7513) and 1% Penicillin Streptomycin (Sigma #P0721)) were detached and placed into plating media (DMEM, 1%FBS and 2mM L-glutamine). 10ml of the HEK293T cells (180,000 cells/ml) were then mixed with 2ml of transfection mix and subsequently seeded into a 96 well poly-D-lysine plate at 100 μ l/well (SLS #356461). Plates were then incubated at 37 °C with 5% CO₂ for 6hrs. Plating media was carefully removed and 100 μ l of assay media added to the wells. Compounds were prepared in 100% DMSO, diluted in media and dosed, making the final assay media volume 150 μ l with compounds at a concentration of 0.15% DMSO. After 48 hours of incubation with compound at 37 °C, 150 μ L of media was

45

removed from each well and frozen, 2HG concentrations were determined subsequently by LC-MS/MS. Cells were fixed in 3% formaldehyde and stained with Hoechst allowing a nuclear count to be performed on the cell insight; 2HG concentrations were normalised to this value.

LC-MS/MS measurement of 2-HG

Media 2-HG was measured by hydrophilic interaction liquid chromatography (HILIC) LC-MS/MS. Cryopreserved media samples were defrosted and diluted 1:10 with water containing deuterated (D3)-2-HG as an internal standard (IS). Solid phase extractions were performed using an Oasis[®] MAX 96-well-plate (Waters, Milford, MA) containing 10mg Oasis MAX sorbent per well. Plates were conditioned with 750μL methanol and 750μL water before buffered test samples were loaded and pulled through under vacuum. Plates were washed with 750μL water and 750μL 50% methanol before extracts were eluted with 2x 250μL 1% formic acid in methanol. Eluates were dried under nitrogen gas, reconstituted in initial conditions (88:2:10 acetonitrile:water:50mM ammonium acetate; pH5.8) and injected into the LC-MS.

Chromatographic separation of 2-HG from co-extracted interferences was performed using high pressure liquid chromatography (Agilent 1200, Agilent) with a Luna HILIC 5uM column (150x3.0mm) (Phenomenex, Torrance, CA). The flow rate was 750uL/min using a gradient starting at 95% mobile phase A, moving to 80% over 180 seconds before rising back to 95% over 60 seconds. This was followed by a hold to equilibrate at 95% phase A for a further 150 seconds. The column temperature was ambient and the sample compartment was chilled to 10°C. Mobile phase A was acetonitrile:50mM ammonium acetate (90:10v/v) pH5.8 and mobile phase B was acetonitrile:water:50mM ammonium acetate (50:40:10v/v/v) pH5.8.

Mass spectrometry detection was made using an API4000 QTrap (AB Sciex, Framingham, MA) operating in negative ion mode with multiple reaction monitoring mass ion transitions 147/85 (2-

1
2
3 HG) and 150/88 (D3-2-HG IS). Data was processed using Analyst Software (Applied
4 Biosystems) and signal intensities obtained by standard peak integration methods. Quantitations
5
6 were performed by comparison against a standard curve generated from multiple dilutions of
7
8 growth medium spiked with 1mM 2-HG stock in water to known concentrations. Final 2-HG
9
10 quantification was derived from a mean of two biological replicates. The lower limit of accurate
11
12 quantification (LLQ) was set at a level twice the peak area measured in conditioned media, to
13
14 ensure robust and confident discrimination of 2-HG from low-level background peaks which
15
16 were observed to co-elute during development of the method.
17
18
19
20
21
22
23

24
25 Generation of stable THP1-IDH1-WT/R132H clones.
26
27

28 Ectopic human IDH1 wild type and IDH1 R132H were stably overexpressed in THP1 AML
29
30 cells using standard site-directed mutagenesis and lentiviral transduction techniques. Briefly, the
31
32 coding sequence of human IDH1 (transcript NCBI accession NM_001282387) was PCR
33
34 amplified from THP1 cDNA with addition of sequence encoding a Myc epitope tag, and ligated
35
36 into the pGEM®T-Easy vector (Promega). Mutant forms were generated by overlap extension
37
38 PCR and expression constructs ligated into the pTRE2minCMV_MCS_SV40_Blast lentiviral
39
40 vector. Lentivirus was generated in 293FT cells using standard techniques, and was used to
41
42 spinoculate THP1 cells previously stably transduced with EF1 α _rtTAadv_IRES_Neo (i.e. the
43
44 tetracycline transactivator component). Successfully transduced cells were selected by culture for
45
46 at least 5 days in 6 μ g/mL blasticidin. Ectopic construct expression was confirmed in lysates by
47
48 Western blotting for the Myc epitope tag and full length IDH1, using standard techniques.
49
50 Vinculin was used as a loading control. Primary antibodies used were: anti-IDH1 (DH21/rabbit;
51
52 Cell Signaling, Beverley MA); anti-MYC-TAG (9B11/mouse; Cell Signaling); anti-VINCULIN
53
54
55
56
57
58
59
60

(hVIN-1/mouse; Sigma Aldrich).

Primary AML patient samples.

Primary material was obtained from bone marrow and peripheral blood samples donated to the Manchester Cancer Research Centre (MCRC) Tissue Biobank, following informed written consent and with approval of the South Manchester Research Ethics Committee. Samples were collected and IDH mutation status was determined as previously described^{31, 32}. Samples selected for use contained $\geq 80\%$ blasts.

Cell culture and clonogenic assays.

Suspension cell lines were cultured in RPMI (Sigma Aldrich) containing 10% tetracycline-free FBS and 1% penicillin/streptomycin (Sigma). Primary AML cells were rapidly thawed in a 37 °C water bath, washed twice in DAMP solution (PBS with 4 μ g/mL DNaseI, 2.5mM MgCl₂, 16.4mM trisodium citrate), and seeded in 200 μ L serum-free StemSpan (Stem Cell Technologies) at 2 x 10⁴ cells per condition in methylcellulose (Methocult H4230; Stem Cell Technologies) final volume 1mL, with the following cytokines at the specified final concentration: IL-3, 20ng/mL; IL-6, 20ng/mL; IL-11, 10ng/mL; FLT3L, 50ng/mL; SCF, 50ng/mL; TPO, 50ng/mL (all from Peprotech); G-CSF, 50ng/mL (Chugai.); and EPO 4U/mL (Janssen Cilag). Compound **20a** or DMSO vehicle was added at 1:1000 for desired final concentration. Plates were cultured at 37 °C and 5% CO₂. After 14 days colonies were scored, counted and photographed before being washed out of methylcellulose by $\geq 10\times$ dilution in PBS and centrifugation. Cells recovered

were subjected to counting by Trypan Blue exclusion and flow cytometry.

Flow cytometry immunophenotyping.

Cells were suspended in staining medium (SM) buffer (5.2g phenol red-free RPMI powder, 15ml FBS, 5ml 1M HEPES, 1ml 500mM EDTA made up to 1L with ddH₂O) with antibodies targeting cell surface markers of myeloid differentiation status. Anti-human antibodies [and clone] used were: anti-CD15-FITC [H198]; anti-CD11b-PE [ICRF44]; and anti-CD117-APC [104D2] (all from Biolegend). All were used at 1:50 concentration. Cells were stained for ≥ 30 minutes in the dark at 4 °C before being re-suspended in fresh SM buffer and analyzed on an LSR FortessaTM flow cytometer (BD Biosciences). Data were analyzed using FlowJo for Mac v10.1r5.

LC-MS/MS measurement of 2-HG. Extracellular and intracellular 2-HG were measured by hydrophilic interaction liquid chromatography (HILIC) LC-MS/MS, on media supernatant removed from cell cultures or cell lysates, respectively. Cryopreserved media samples were defrosted and diluted 1:10 with water containing deuterated (D₃)-2-HG as an internal standard (IS). Solid phase extractions were performed using an Oasis[®] MAX 96-well-plate (Waters) containing 10mg Oasis MAX sorbent per well. Plates were conditioned with 750 μ L methanol and 750 μ L water before buffered test samples were loaded and pulled through under vacuum. Plates were washed with 750 μ L water, 750 μ L 50% methanol and 100% methanol before extracts were eluted with 2x 250 μ L 1% formic acid in methanol. For cell lysates, pelleted cells were washed twice with ice-cold PBS before sequential quenching with -80 °C 80% methanol:20%

water containing 0.5µg/mL D3-2-HG IS; transfer to dry ice bed; sonication on a Biorupter® (Diagenode) at high power for 5 minutes (at 30 secs on/30 secs off); and subsequent incubation at -80 °C for ≥40 minutes. Debris was removed by centrifugation at 14,000xg and supernatant was used for LC-MS/MS. Eluates were dried under nitrogen gas, reconstituted in initial conditions (88:2:10 acetonitrile:water:50mM ammonium acetate; pH5.8) and injected into the LC-MS.

Chromatographic separation of 2-HG from co-extracted interferences was performed using high pressure liquid chromatography (Agilent 1200, Agilent) with a Luna HILIC 5µM column (150x3.0mm) (Phenomenex). The flow rate was 750µL/min using a gradient starting at 95% mobile phase A, moving to 80% over 180 seconds before rising back to 95% over 60 seconds. This was followed by a hold to equilibrate at 95% phase A for a further 150 seconds. The column temperature was ambient and the sample compartment was chilled to 10°C. Mobile phase A was acetonitrile:50mM ammonium acetate (90:10v/v) pH5.8 and mobile phase B was acetonitrile:water:50mM ammonium acetate (50:40:10v/v/v) pH5.8.

Mass spectrometry detection was made using an API4000 QTrap (AB Sciex) operating in negative ion mode with multiple reaction monitoring mass ion transitions 147/85 (2-HG) and 150/88 (D3-2-HG IS). Data was processed using Analyst Software (Applied Biosystems) and signal intensities obtained by standard peak integration methods. Quantitations were performed by comparison against a standard curve generated from multiple dilutions of growth medium spiked with 1mM 2-HG stock in water to known concentrations. Final 2-HG quantification was derived from a mean of two biological replicates. The lower limit of accurate quantification (LLQ) was set at a level twice the peak area measured in conditioned media, to ensure robust and

confident discrimination of 2-HG from low-level background peaks which were observed to co-elute during development of the method.

IDH1 Cloning & mutagenesis

IDH1 (NP_005887) cDNA was cloned into the NdeI and EcoRI sites of bacterial expression vector pET22b (Merck). Disease mutation R132H was first introduced by site directed mutagenesis using the following oligos: Top 5' GATTATCATTGGTCATCATGCCTATG 3' and Bottom 3' CATAGGCATGATGACCAATGATAATC 5'. Surface mutations E80A and K81A were introduced using oligos: Top 5' GCGCGACCATACGCCGGATGCAGCACGTGTGGAAGAATTCAAAC-3' and Bottom 3'GTTTGAATTCTTCCACACGTGCTGCATCCGGCGTAATGGTCGCGC-5'. Surface mutations E240A, Q242A and K243A were then produced using oligos: Top 5'GTACAAAAGCCAGTTTGCAGCGGCGGCAATCTGGTATGAACATCG 3' and Bottom 3'CGATGTTTCATACCAGATTGCCGCCGCTGCAAACCTGGCTTTTGTAC 5'. Site Directed mutations were made using a two-step PCR method using Phusion HF enzyme (NEB). Step 1 involved single top or bottom primer PCR reactions and these were then combined 50:50 in step 2. Reaction conditions were Step1: 98 °C 1 min, followed by 10 cycles of 98 °C 10 sec, 55 °C 30 sec, 72 °C 5 min. Step2: 98 °C 1 min followed by 18 cycles of 98 °C 10 sec, 55 °C 30 sec, 72 °C 5 min then 72 °C 10 min and 4 °C hold. PCR reactions were DpnI digested (Fermentas) and transformed into DH5a competent cells (NEB). Colonies were selected for miniprep analysis (Qiagen) and constructs sequenced confirmed (Stopford Sequencing Facility, Manchester University).

Protein expression and purification for crystallography.

pET22b: IDH1 R132H, E80A, K81A, E240A, Q242A, K243A mutation construct was freshly transformed every time into JM109 (DE3) *E.Coli* cells and selected on LB ampicillin agar plate (100ug/ml). Culture was grown to an OD_{600nm} of ~0.6 and induced by 0.2mM IPTG with shaking at 30 °C for 20hrs. Pelleted cells were lysed in 50mM Tris-HCL, pH8.0, 300mM NaCl and 2% glycerol buffer containing protease inhibitor cocktail (Sigma, EDTA free), 5mM imidazole and 1% Triton X-100 (TX100) then sonicated for 7x20 sec on/off on ice (setting 20%). The lysate was clarified at 17,000 rpm, 30 min @ 4°C and bound in batch to Nickel NTA beads (Qiagen) and washed to 20mM Imidazole stringency in lysis buffer lacking TX100. Bound protein was eluted in 250mM Imidazole, 50mM Tris-HCl pH 8.0, 100mM NaCl, 2% glycerol buffer. The protein sample was concentrated down to at least 1.6ml using a Vivaspin20 MWCO 5,000 column and injected onto a HiLoad 16/60 Superdex 200 pg gel filtration (GF) column (GE Healthcare) and the separation run at 4 °C against 50mM Tris-HCl pH 8.0, 100mM NaCl without glycerol. For substrate binding, NADP substrate to [0.5mM] (Sigma) was added to the dilute GF purified protein for 30 min on ice, clarified by spinning at 4.5Krpm for 10 min at 4 °C before concentrating using a Vivaspin 6 or 20 MWCO 3,000 (Generon) to >10mg/ml. For ligand complexing, the dilute GF purified protein was incubated overnight at 4 °C on a roller with an excess of dry compound. The protein was clarified by spinning at 4.5Krpm for 10 min at 4 °C and concentrated to >10mg/ml. All protein concentration estimations were carried out by Bradford analysis using BSA standards (Biorad).

Crystallisation and Structure Determination

A sample of apo protein was prepared 24 hours prior to the ligand complexes and used to obtain crystals for seeding purposes. All crystals were obtained by the sitting drop vapour diffusion method. Apo crystals were grown by mixing 200nl of protein with 200nl of a reservoir solution of 0.06M Divalents, 0.1M Tris / Bicine pH 8.5, 50% (40% v/v PEG 500 MME, 20% w/v PEG 20K) [Morpheus E9]. CocrySTALLISATION trials with compound **9** and **20a** were setup with 180nl of protein, 20nl of apo crystal seed stock and 200nl of reservoir solution. All plates were incubated overnight at 4 °C prior to manual inspection. Single crystals of compound **9** were obtained from the same reservoir solution as described above for the apo crystals [Morpheus E9]. Single crystals of compound **20a** were obtained from a reservoir solution of 0.12M Ethylene Glycols, 0.1M Bicine pH 8.5, 50% (40% v/v PEG 500 MME, 20% w/v PEG 20K) [Morpheus A9].

Single cocrySTALS of IDH1 R132H **9/20a** were flash cooled by immersion in liquid nitrogen prior to X-ray data collection at the Diamond Light Source, Oxford, UK. All data were subsequently scaled and merged with XDS. Structures were determined by molecular replacement with phenix.phaser³³ and models rebuilt and refined through iterative cycles of COOT³⁴ and phenix.refine. Validation with MolProbity³⁵ and PDB_REDO³⁶ were integrated into the iterative rebuild and refinement procedure. Data collection and refinement statistics are presented in Supplementary Data Table S2

ASSOCIATED CONTENT

* Supporting Information

Summary of LC–MS methods and solvent gradients; preparative HPLC instrument and solvent gradients; purity data, detailed chemical experimental for all compounds described, selected ^1H and ^{13}C NMR spectra, protein purification and crystallographic methods. This material is available free of charge via the Internet at <http://pubs.acs.org>.

AUTHOR INFORMATION

*Corresponding Author

Telephone: +44(0)161 446 8079. E-mail: Allan.Jordan@cruk.manchester.ac.uk.

Notes

The authors declare no competing financial interest.

[∞] These authors contributed equally to this work.

ACKNOWLEDGMENTS

This work was funded by Cancer Research UK (Grant numbers C480/A1141, C5759/A17098 and C5759/A20971). HTS hit output, analysis and helpful advice were kindly provided through a collaborative research agreement with AstraZeneca. Dan Wiseman is supported by a Bloodwise Clinician Scientist Fellowship (15030), The Oglesby Leukaemia Clinical Research Fellowship, and has received additional support from Cancer Research UK. In vitro DMPK data were provided by Cyprotex Discovery. JChem for Excel was used for structure property prediction and calculation and general data handling (JChem for Excel, version 6.1.5.781, 2008–2013, ChemAxon (<http://www.chemaxon.com>)).

We thank Diamond Light Source for access to beamlines i04 & i04-1 (MX-8997) that contributed to the results presented here.

Ligand interaction diagrams in Figures 4, 7 and 8 were generated within Maestro and images of protein-ligand complexes within the PyMOL Molecular Graphics System (Schrödinger, LLC).

ABBREVIATIONS

IDH – isocitrate dehydrogenase; AML – acute myeloid Leukemia; NADP – nicotinamide adenine dinucleotide phosphate; α -KG – α ketoglutarate; 2-HG – 2-hydroxyglutarate ;TET2 – Tet methylcytosine dioxygenase 2; DNA – Deoxyribonucleic acid; ICT – isocitrate; AZ – Astrazeneca; CRUK-MI – Cancer Research UK – Manchester Institute; HTS – High throughput screen; SPR – surface plasmon resonance; 11 β -HSD1 – 11 β -hydroxysteroid dehydrogenase Type 1; PDB – Protein Databank; SAR –Structure activity relationship; DIPEA – diisopropyl ethylamine; HPLC – High performance liquid chromatography; NMR – Nuclear magnetic resonance; G6PD – glucose-6-phosphate dehydrogenase; DMSO – dimethyl sulfoxide; THF – tetrahydrofuran; DCM – dichloromethane; LCMS – Liquid chromatography-mass spectrometry; DMF – dimethylformamide; EtOAc – ethyl acetate.

PDB ID Codes: 5L57, 5L58. Authors will release the atomic coordinates and experimental data upon article publication.

REFERENCES

1. Parsons, D. W.; Jones, S.; Zhang, X.; Lin, J. C.; Leary, R. J.; Angenendt, P.; Mankoo, P.; Carter, H.; Siu, I. M.; Gallia, G. L.; Olivi, A.; McLendon, R.; Rasheed, B. A.; Keir, S.; Nikolskaya, T.; Nikolsky, Y.; Busam, D. A.; Tekleab, H.; Diaz, L. A., Jr.; Hartigan, J.; Smith, D. R.; Strausberg, R. L.; Marie, S. K.; Shinjo, S. M.; Yan, H.; Riggins, G. J.; Bigner, D. D.; Karchin, R.; Papadopoulos, N.; Parmigiani, G.; Vogelstein, B.; Velculescu, V. E.; Kinzler, K. W. An integrated genomic analysis of human glioblastoma multiforme. *Science* **2008**, *321*, 1807-1812.

2. Marcucci, G.; Maharry, K.; Wu, Y. Z.; Radmacher, M. D.; Mrozek, K.; Margeson, D.; Holland, K. B.; Whitman, S. P.; Becker, H.; Schwind, S.; Metzeler, K. H.; Powell, B. L.; Carter, T. H.; Kolitz, J. E.; Wetzler, M.; Carroll, A. J.; Baer, M. R.; Caligiuri, M. A.; Larson, R. A.; Bloomfield, C. D. IDH1 and IDH2 gene mutations identify novel molecular subsets within de novo cytogenetically normal acute myeloid leukemia: a Cancer and Leukemia Group B study. *J. Clin. Oncol.* **2010**, *28*, 2348-2355.
3. Wagner, K.; Damm, F.; Gohring, G.; Gorlich, K.; Heuser, M.; Schafer, I.; Ottmann, O.; Lubbert, M.; Heit, W.; Kanz, L.; Schlimok, G.; Raghavachar, A. A.; Fiedler, W.; Kirchner, H. H.; Brugger, W.; Zucknick, M.; Schlegelberger, B.; Heil, G.; Ganser, A.; Krauter, J. Impact of IDH1 R132 mutations and an IDH1 single nucleotide polymorphism in cytogenetically normal acute myeloid leukemia: SNP rs11554137 is an adverse prognostic factor. *J. Clin. Oncol.* **2010**, *28*, 2356-2364.
4. Gupta, R.; Flanagan, S.; Li, C. C.; Lee, M.; Shivalingham, B.; Maleki, S.; Wheeler, H. R.; Buckland, M. E. Expanding the spectrum of IDH1 mutations in gliomas. *Mod. Pathol.* **2013**, *26*, 619-625.
5. Dang, L.; White, D. W.; Gross, S.; Bennett, B. D.; Bittinger, M. A.; Driggers, E. M.; Fantin, V. R.; Jang, H. G.; Jin, S.; Keenan, M. C.; Marks, K. M.; Prins, R. M.; Ward, P. S.; Yen, K. E.; Liao, L. M.; Rabinowitz, J. D.; Cantley, L. C.; Thompson, C. B.; Vander Heiden, M. G.; Su, S. M. Cancer-associated IDH1 mutations produce 2-hydroxyglutarate. *Nature* **2009**, *462*, 739-744.
6. Ward, P. S.; Patel, J.; Wise, D. R.; Abdel-Wahab, O.; Bennett, B. D.; Collier, H. A.; Cross, J. R.; Fantin, V. R.; Hedvat, C. V.; Perl, A. E.; Rabinowitz, J. D.; Carroll, M.; Su, S. M.; Sharp, K. A.; Levine, R. L.; Thompson, C. B. The common feature of leukemia-associated IDH1 and IDH2 mutations is a neomorphic enzyme activity converting alpha-ketoglutarate to 2-hydroxyglutarate. *Cancer Cell* **2010**, *17*, 225-234.
7. Clark, O.; Yen, K.; Mellinghoff, I. K. Molecular pathways: isocitrate dehydrogenase mutations in Cancer. *Clin. Cancer Res.* **2016**, *22*, 1837-1842.

8. Zhao, S.; Guan, K. L. IDH1 mutant structures reveal a mechanism of dominant inhibition. *Cell Res.* **2010**, *20*, 1279-1281.
9. Figueroa, M. E.; Abdel-Wahab, O.; Lu, C.; Ward, P. S.; Patel, J.; Shih, A.; Li, Y.; Bhagwat, N.; Vasanthakumar, A.; Fernandez, H. F.; Tallman, M. S.; Sun, Z.; Wolniak, K.; Peeters, J. K.; Liu, W.; Choe, S. E.; Fantin, V. R.; Paietta, E.; Lowenberg, B.; Licht, J. D.; Godley, L. A.; Delwel, R.; Valk, P. J.; Thompson, C. B.; Levine, R. L.; Melnick, A. Leukemic IDH1 and IDH2 mutations result in a hypermethylation phenotype, disrupt TET2 function, and impair hematopoietic differentiation. *Cancer Cell* **2010**, *18*, 553-567.
10. Xu, W.; Yang, H.; Liu, Y.; Yang, Y.; Wang, P.; Kim, S. H.; Ito, S.; Yang, C.; Wang, P.; Xiao, M. T.; Liu, L. X.; Jiang, W. Q.; Liu, J.; Zhang, J. Y.; Wang, B.; Frye, S.; Zhang, Y.; Xu, Y. H.; Lei, Q. Y.; Guan, K. L.; Zhao, S. M.; Xiong, Y. Oncometabolite 2-hydroxyglutarate is a competitive inhibitor of alpha-ketoglutarate-dependent dioxygenases. *Cancer Cell* **2011**, *19*, 17-30.
11. Turcan, S.; Rohle, D.; Goenka, A.; Walsh, L. A.; Fang, F.; Yilmaz, E.; Campos, C.; Fabius, A. W.; Lu, C.; Ward, P. S.; Thompson, C. B.; Kaufman, A.; Guryanova, O.; Levine, R.; Heguy, A.; Viale, A.; Morris, L. G.; Huse, J. T.; Mellinghoff, I. K.; Chan, T. A. IDH1 mutation is sufficient to establish the glioma hypermethylator phenotype. *Nature* **2012**, *483*, 479-483.
12. Yang, H.; Ye, D.; Guan, K. L.; Xiong, Y. IDH1 and IDH2 mutations in tumorigenesis: mechanistic insights and clinical perspectives. *Clin. Cancer Res.* **2012**, *18*, 5562-5571.
13. Dang, L.; Yen, K.; Attar, E. C. IDH mutations in cancer and progress toward development of targeted therapeutics. *Ann. Oncol.* **2016**, *27*, 599-608.
14. Popovici-Muller, J.; Saunders, J. O.; Salituro, F. G.; Travins, J. M.; Yan, S.; Zhao, F.; Gross, S.; Dang, L.; Yen, K. E.; Yang, H.; Straley, K. S.; Jin, S.; Kunii, K.; Fantin, V. R.; Zhang, S.; Pan, Q.; Shi, D.; Biller, S. A.; Su, S. M. Discovery of the first potent inhibitors of mutant IDH1 that lower tumor 2-HG in vivo. *ACS Med. Chem. Lett.* **2012**, *3*, 850-855.

15. Rohle, D.; Popovici-Muller, J.; Palaskas, N.; Turcan, S.; Grommes, C.; Campos, C.; Tsoi, J.; Clark, O.; Oldrini, B.; Komisopoulou, E.; Kunii, K.; Pedraza, A.; Schalm, S.; Silverman, L.; Miller, A.; Wang, F.; Yang, H.; Chen, Y.; Kernysky, A.; Rosenblum, M. K.; Liu, W.; Biller, S. A.; Su, S. M.; Brennan, C. W.; Chan, T. A.; Graeber, T. G.; Yen, K. E.; Mellinghoff, I. K. An inhibitor of mutant IDH1 delays growth and promotes differentiation of glioma cells. *Science* **2013**, *340*, 626-630.
16. Zheng, B.; Yao, Y.; Liu, Z.; Deng, L.; Anglin, J. L.; Jiang, H.; Prasad, B. V.; Song, Y. Crystallographic investigation and selective inhibition of mutant isocitrate dehydrogenase. *ACS Med. Chem. Lett.* **2013**, *4*, 542-546.
17. Davis, M. I.; Gross, S.; Shen, M.; Straley, K. S.; Pragani, R.; Lea, W. A.; Popovici-Muller, J.; DeLaBarre, B.; Artin, E.; Thorne, N.; Auld, D. S.; Li, Z.; Dang, L.; Boxer, M. B.; Simeonov, A. Biochemical, cellular, and biophysical characterization of a potent inhibitor of mutant isocitrate dehydrogenase IDH1. *J. Biol. Chem.* **2014**, *289*, 13717-13725.
18. Cho, Y. S. L.; J. R.; Toure, B.; Yang, F.; Caferro, T.; Lei, H.; Lenoir, F.; Liu, G.; Palermo, M. G.; Shultz, M. D.; Smith, T.; Costales, A. Q.; Pfister, K. B.; Sendzik, M.; Shafer, C.; Sutton, J.; Zhao, Q. 3-Pyrimidin-4-yl-oxazolidin-2-ones as inhibitors of mutant IDH. WO2013046136, 2013.
19. Brooks, E.; Wu, X.; Hanel, A.; Nguyen, S.; Wang, J.; Zhang, J. H.; Harrison, A.; Zhang, W. Identification and characterization of small-molecule inhibitors of the R132H/R132H mutant isocitrate dehydrogenase 1 homodimer and R132H/wild-type heterodimer. *J. Biomol. Screening* **2014**, *19*, 1193-1200.
20. Deng, G.; Shen, J.; Yin, M.; McManus, J.; Mathieu, M.; Gee, P.; He, T.; Shi, C.; Bedel, O.; McLean, L. R.; Le-Strat, F.; Zhang, Y.; Marquette, J. P.; Gao, Q.; Zhang, B.; Rak, A.; Hoffmann, D.; Rooney, E.; Vassort, A.; Englaro, W.; Li, Y.; Patel, V.; Adrian, F.; Gross, S.; Wiederschain, D.; Cheng, H.; Licht, S. Selective inhibition of mutant isocitrate dehydrogenase 1 (IDH1) via disruption of a metal binding network by an allosteric small molecule. *J. Biol. Chem.* **2015**, *290*, 762-774.

21. Liu, Z.; Yao, Y.; Kogiso, M.; Zheng, B.; Deng, L.; Qiu, J. J.; Dong, S.; Lv, H.; Gallo, J. M.; Li, X. N.; Song, Y. Inhibition of cancer-associated mutant isocitrate dehydrogenases: synthesis, structure-activity relationship, and selective antitumor activity. *J. Med. Chem.* **2014**, *57*, 8307-8318.
22. Wu, F.; Jiang, H.; Zheng, B.; Kogiso, M.; Yao, Y.; Zhou, C.; Li, X. N.; Song, Y. Inhibition of cancer-associated mutant isocitrate dehydrogenases by 2-thiohydantoin compounds. *J. Med. Chem.* **2015**, *58*, 6899-6908.
23. Okoye-Okafor, U. C.; Bartholdy, B.; Cartier, J.; Gao, E. N.; Pietrak, B.; Rendina, A. R.; Rominger, C.; Quinn, C.; Smallwood, A.; Wiggall, K. J.; Reif, A. J.; Schmidt, S. J.; Qi, H.; Zhao, H.; Joberty, G.; Faelth-Savitski, M.; Bantscheff, M.; Drewes, G.; Duraiswami, C.; Brady, P.; Groy, A.; Narayanagari, S. R.; Antony-Debre, I.; Mitchell, K.; Wang, H. R.; Kao, Y. R.; Christopeit, M.; Carvajal, L.; Barreyro, L.; Paietta, E.; Makishima, H.; Will, B.; Concha, N.; Adams, N. D.; Schwartz, B.; McCabe, M. T.; Maciejewski, J.; Verma, A.; Steidl, U. New IDH1 mutant inhibitors for treatment of acute myeloid leukemia. *Nat. Chem. Biol.* **2015**, *11*, 878-886.
24. Rehwinkel, H.; Panknin, O.; Ring, S.; Anlauf, S.; Siebeneicher, H.; Nguyen, D.; Schede, W.; Bauser, M.; Zimmermann, K.; Kaulfuss, S.; Neuhaus, R.; Blaney, P. Benzimidazol-2-amines as mIDH1 inhibitors. WO2015121210, 2015
25. Yang, B.; Zhong, C.; Peng, Y.; Lai, Z.; Ding, J. Molecular mechanisms of "off-on switch" of activities of human IDH1 by tumor-associated mutation R132H. *Cell Res.* **2010**, *20*, 1188-1200.
26. Scott, J. S.; Bowker, S. S.; Deschoolmeester, J.; Gerhardt, S.; Hargreaves, D.; Kilgour, E.; Lloyd, A.; Mayers, R. M.; McCoull, W.; Newcombe, N. J.; Ogg, D.; Packer, M. J.; Rees, A.; Revill, J.; Schofield, P.; Selmi, N.; Swales, J. G.; Whittamore, P. R. Discovery of a potent, selective, and orally bioavailable acidic 11 β -hydroxysteroid dehydrogenase type 1 (11 β -HSD1) inhibitor: discovery of 2-[(3S)-1-[5-(cyclohexylcarbamoyl)-6-propylsulfanylpiperidin-2-yl]-3-piperidyl]acetic acid (AZD4017). *J. Med. Chem.* **2012**, *55*, 5951-5964.

27. Merk, A.; Bartesaghi, A.; Banerjee, S.; Falconieri, V.; Rao, P.; Davis, M. I.; Pragani, R.; Boxer, M. B.; Earl, L. A.; Milne, J. L.; Subramaniam, S. Breaking cryo-EM resolution Barriers to facilitate drug discovery. *Cell* **2016**, *165*, 1698-1707.
28. Wang, F.; Travins, J.; DeLaBarre, B.; Penard-Lacronique, V.; Schalm, S.; Hansen, E.; Straley, K.; Kernysky, A.; Liu, W.; Gliser, C.; Yang, H.; Gross, S.; Artin, E.; Saada, V.; Mylonas, E.; Quivoron, C.; Popovici-Muller, J.; Saunders, J. O.; Salituro, F. G.; Yan, S.; Murray, S.; Wei, W.; Gao, Y.; Dang, L.; Dorsch, M.; Agresta, S.; Schenkein, D. P.; Biller, S. A.; Su, S. M.; de Botton, S.; Yen, K. E. Targeted inhibition of mutant IDH2 in leukemia cells induces cellular differentiation. *Science* **2013**, *340*, 622-626.
29. Dinardo, C. d. B., S.; Pollyea, D. A.; Stein, E. M.; Fathi, A. T.; Roboz, G. J.; Collins, R.; Swords, R. T.; Flinn, I. W.; Altman, J. K.; Tallman, M. S.; Kantarjian, H. M.; Derti, A.; Goldwasser, M.; Prah, M.; Wu, B.; Yen, K.; Agresta, S.; Stone, R. M. Molecular profiling and relationship with clinical response in patients with IDH1 mutation-positive hematologic malignancies receiving AG-120, a first-in-class potent inhibitor of mutant IDH1, in addition to data from the completed dose escalation portion of the phase 1 study (Abstract). *Blood* **2015**, *126*, 1306.
30. Stein, E. M.; Tallman, M. S. Emerging therapeutic drugs for AML. *Blood* **2016**, *127*, 71-8.
31. Wiseman, D. H.; Small, H. F.; Wilks, D. P.; Waddell, I. D.; Dennis, M. W.; Ogilvie, D. J.; Somervaille, T. C. Elevated plasma 2-hydroxyglutarate in acute myeloid leukaemia: association with the IDH1 SNP rs11554137 and severe renal impairment. *Br. J. Haematol.* **2014**, *166*, 145-148.
32. Wiseman, D. H.; Struys, E. A.; Wilks, D. P.; Clark, C. I.; Dennis, M. W.; Jansen, E. E.; Salomons, G. S.; Somervaille, T. C. Direct comparison of quantitative digital PCR and 2-hydroxyglutarate enantiomeric ratio for IDH mutant allele frequency assessment in myeloid malignancy. *Leukemia* **2015**, *29*, 2421-2423.
33. Adams, P. D.; Afonine, P. V.; Bunkoczi, G.; Chen, V. B.; Davis, I. W.; Echols, N.; Headd, J. J.; Hung, L. W.; Kapral, G. J.; Grosse-Kunstleve, R. W.; McCoy, A. J.; Moriarty, N. W.; Oeffner, R.; Read, R. J.; Richardson, D. C.; Richardson, J. S.; Terwilliger, T. C.; Zwart, P. H. PHENIX: a comprehensive

Python-based system for macromolecular structure solution. *Acta Crystallogr., Sect. D: Biol. Crystallogr.* **2010**, *66*, 213-221.

34. Emsley, P.; Cowtan, K. Coot: model-building tools for molecular graphics. *Acta Crystallogr., Sect. D: Biol. Crystallogr.* **2004**, *60*, 2126-2132.

35. Chen, V. B.; Arendall, W. B., 3rd; Headd, J. J.; Keedy, D. A.; Immormino, R. M.; Kapral, G. J.; Murray, L. W.; Richardson, J. S.; Richardson, D. C. MolProbity: all-atom structure validation for macromolecular crystallography. *Acta Crystallogr., Sect. D: Biol. Crystallogr.* **2010**, *66*, 12-21.

36. Joosten, R. P.; Long, F.; Murshudov, G. N.; Perrakis, A. The PDB_REDO server for macromolecular structure model optimization. *IUCrJ* **2014**, *1*, 213-220.

Picture for graphical abstract

